

Excessive Long-Time Deflections of Prestressed Box Girders. I: Record-Span Bridge in Palau and Other Paradigms

Zdeněk P. Bažant, Hon.M.ASCE¹; Qiang Yu²; and Guang-Hua Li³

Abstract: The segmental prestressed concrete box girder of Koror-Babeldaob (KB) Bridge in Palau, which had a record span of 241 m (791 ft), presents a striking paradigm of serviceability loss because of excessive multidecade deflections. The data required for analysis have recently been released and are here exploited to show how the analysis and design could be improved. Erected segmentally in 1977, this girder developed a midspan deflection of 1.61 m (5.3 ft) compared with the design camber after 18 years, and it collapsed in 1996 as a consequence of remedial prestressing, after a 3-month delay. Compared with three-dimensional analysis, the traditional beam-type analysis of box girder deflections is found to have errors up to 20%, although greater errors are likely for bridges with higher box-width-to-span ratios than the KB Bridge. However, even three-dimensional finite-element analysis with step-by-step time integration cannot explain the observed deflections when the current American Concrete Institute, Japan Society of Civil Engineers, Comité Euro-International du Béton (or Comité Euro-International du Béton—Fédération internationale de la précontrainte), and Gardner and Lockman prediction models for creep and shrinkage are used. These models give 18-year deflection estimates that are 50–77% lower than measured and yield unrealistic shapes of the deflection history. They also predict the 18-year prestress loss to be 46–56% lower than the measured mean prestress loss, which was 50%. Model B3, which is the only theoretically based model, underestimates the 18-year deflection by 42% and gives a prestress loss of 40% when the default parameter values are used. However, in Model B3, several input parameters are adjustable and if they are adjusted according to the long-time laboratory tests of Brooks, a close fit of all the measurements is obtained. For early deflections and their extrapolation, it is important that Model B3 can capture realistically the differences in the rates of shrinkage and drying creep caused by the differences in the thickness of the walls of the cross section. The differences in temperature and possible cracking of the top slab also need to be taken into account. Other paradigms on which data have recently been released are four bridges in Japan and one in the Czech Republic. Their excessive deflections can also be explained. The detailed method of analysis and the lessons learned are presented in Part II. DOI: [10.1061/\(ASCE\)ST.1943-541X.0000487](https://doi.org/10.1061/(ASCE)ST.1943-541X.0000487). © 2012 American Society of Civil Engineers.

CE Database subject headings: Creep; Shrinkage; Box girders; Serviceability; Deflection; Span bridges.

Author keywords: Prestressed box girder; Bridges; Segmental erection; Shear lag; Design standards; Concrete; Relaxation.

Introduction

Clarification of the causes of major disasters and serviceability loss has been and will always be a prime opportunity for progress in structural engineering. A paradigm that presents such an opportunity for creep and shrinkage analysis and design is offered by the excessive deflections of the Koror-Babeldaob (KB) Bridge, which crossed the Toegel Channel between the islands of Koror and Babeldaob in the Republic of Palau in the tropical western Pacific [Fig. 1(a)]. When it was completed in 1977, its main span of 241 m (791 ft) set the world

record for segmental prestressed concrete box girders (Yee 1979). The final deflection, measured as the difference from the design camber of -0.3 m (or -12 in.), was expected to terminate at 0.76 – 0.88 m (30 – 34.6 in.), as predicted by the design (ABAM 1993; Khaled Shawwaf, personal communication, September, 18, 2008) based on the original CEB-FIP design recommendations (1970–1972). According to the 1971 American Concrete Institute (ACI) model (ACI 1971), which is still in force today (reapproved in 2008) (ACI 2008a), the deflection measured from the design camber would have been predicted as 0.71 m (28 in.) according to McDonald et al. (2003) and 0.737 m (29 in.) according to the present analysis.

After 18 years, the deflection measured at the end of the construction reached 1.39 m (54.7 in.) and kept growing (ABAM 1993; Berger/ABAM 1995a). The design camber of 0.30 m (12 in.) was not met (Khaled Shawwaf, personal communication, September 18, 2008) and an additional creep deflection of 0.22 m (9 in.) had accumulated during the segmental erection, making the actual camber only 0.075 m (3 in.) when the cantilevers were joined. Thus, the total 18-year deflection at midspan was 1.61 m (5.3 ft).

Remedial prestressing was undertaken but caused the bridge to collapse (after a 3-month delay) on September 26, 1996, with two fatalities and many injuries (SSF 1996; Parker 1996; Pilz 1997, 1999; McDonald et al. 2003; Burgoyne and Scantlebury 2006) [see Fig. 1(b)].

¹McCormick Institute Professor and W. P. Murphy Professor of Civil Engineering and Materials Science, Dept. of Civil and Environmental Engineering, Northwestern Univ., 2145 Sheridan Rd., CEE/A135, Evanston, IL 60208 (corresponding author). E-mail: z-bazant@northwestern.edu

²Assistant Professor, Dept. of Civil Engineering, Univ. of Pittsburgh, PA; formerly, Postdoctoral Research Associate, Northwestern Univ., Evanston, IL 60208.

³Graduate Research Assistant, Northwestern Univ., Evanston, IL 60208.

Note. This manuscript was submitted on February 1, 2010; approved on August 1, 2011; published online on May 15, 2012. Discussion period open until November 1, 2012; separate discussions must be submitted for individual papers. This paper is part of the *Journal of Structural Engineering*, Vol. 138, No. 6, June 1, 2012. ©ASCE, ISSN 0733-9445/2012/6-676-686/\$25.00.



Fig. 1. (a) Koror-Babeldaob Bridge in Palau (in 1977); (b) Babeldaob side after the collapse (in 1996) (images courtesy DYWIDAG Systems International and Wiss, Janney, Elstner Associates, Inc., with permission)

As a result of the legal litigation, the technical data collected by the investigating agencies in relation to this major disaster were unavailable to the engineering public for many years. A worldwide group of 47 experts (see the Appendix), therefore proposed a resolution at the Third Structural Engineers World Congress in Bangalore that called, on the grounds of engineering ethics, for the release of all technical data necessary for analyses of major structural collapses, including the bridge in Palau. The resolution passed on November 6, 2007, and was circulated widely. In January 2008, the Attorney General of the Republic of Palau permitted the release of the necessary technical data.

The present two-part study (see also Bažant et al. 2012), which updates a 2008 preliminary report (Bažant et al. 2008) and expands a brief recent article (Bažant et al. 2010), aims to explain the reasons for the excessive long-term deflections and compare the performance of various existing models. Understanding the reasons is important because recent data collection (Bažant et al. 2011a, b, c) has revealed similar, mostly excessive, deflections of 69 similar bridge spans (and likely many more). The method of analysis is presented in detail in Part II (Bažant et al. 2012), which also enunciates the lessons for structural analysis and design. Hopefully, these lessons will resolve the currently intractable disagreements in technical committees about the optimal prediction model that can be used as a standard guide. These lessons should also help interpret the health monitoring of structures. Clarification of the collapse caused by remedial prestressing will be postponed for a subsequent article. A forthcoming article (Yu et al. 2012) further makes a comparison with a popular commercial bridge creep program (SOFiSTiK).

Bridge Description and Input Data for Analysis

The main span of 241 m (791 ft) consisted of two symmetric concrete cantilevers connected at midspan by a horizontally sliding hinge. Each cantilever consisted of 25 cast-in-place segments of depths varying from 14.17 m (46.5 ft) at the main piers to 3.66 m (12 ft) at the midspan. The main span was flanked by 72.2 m (237 ft) long side spans in which the box girder was partially filled with rock ballast to balance the moment at the main pier. The total length of the bridge was 386 m (1,266 ft). The thickness of the top slab ranged from 432 mm (17 in.) at the main piers to 280 mm (11 in.) at the midspan. The thickness of the bottom slab varied from 1,153 mm (45.4 in.) at the main piers to 178 mm (7 in.) at the midspan. Compared with the depth of the girder, the webs had an unusually small thickness of 356 mm (14 in.), which was constant throughout the whole main span. The typical cross sections are shown in Fig. 2.

Type I portland cement was used for the superstructure (Khaled Shawwaf, personal communication, September, 18, 2008). The mass density of the concrete was $\rho = 2,325 \text{ kg/m}^3$ (145 lb/ft³).

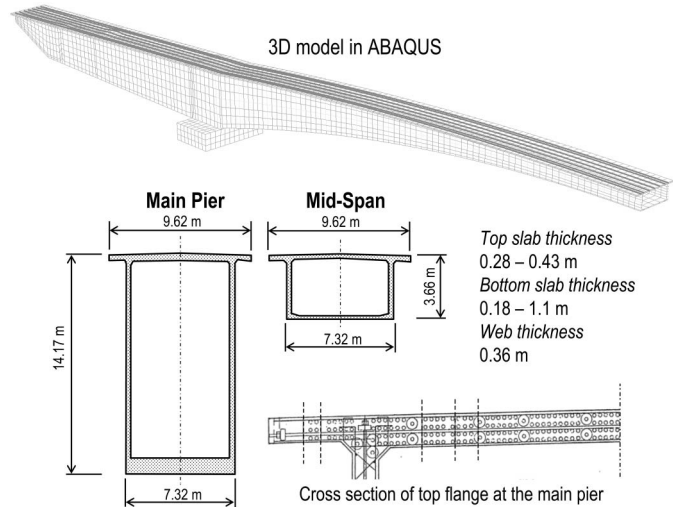


Fig. 2. 3D view of one-half of the box girder, its cross sections at the main pier and at the middle of the main span, and the placement of prestressing tendons at the main pier

The top slab was covered by concrete pavement with an average thickness of 76 mm (3 in.) and a density of 2,233 kg/m³ (139 lb/ft³). The aggregate was crushed basalt rock of the maximum aggregate size of approximately 19 mm (3/4 in), supplied from a quarry on the island of Malakal. Beach sand from Palau was used as the fine aggregate, and its washing by mechanical means helped keep the chloride content within the limit allowed (Berger/ABAM 1995b).

Although no original measurements of the Young's elastic modulus E_c of the concrete are known, some information was obtained in 1990 through core sample tests (JICA 1990). These tests yielded $E_c = 22.1 \text{ GPa}$ (3,200 ksi). In 1995, further core sample tests (Berger/ABAM 1995a) made just before the retrofit revealed the porosity to be high and E_c to be approximately 21.7 GPa (3,150 ksi). Both investigations showed values approximately 23% lower than the value estimated from the design compression strength according to the ACI empirical formula, which is 28.3 GPa (4,110 ksi). Truck load tests were conducted during an on-site investigation by the Japan International Cooperation Agency (JICA). Matching the deflections measured at midspan by finite-element elastic analysis provided, after a correction for concrete age according to the ACI formula, an average 28-day E_c of approximately 22.0 GPa (3,190 ksi) (JICA 1990). This E_c value was adopted for analysis because the load test gives the average elastic modulus in the box girder.

The prestress was generated by Dywidag threaded alloy bars (tendons) [yield strength 1,034 MPa (150 kip); diameter

31.8 mm (1.25 in.), extended by couplers, anchored by nuts, and grouted in ducts [diameter 47.6 mm (1.9 in.)] (ABAM 1993; DRC 1996). Some tendons were stressed from one end and some from both ends (Yee 1979; McDonald et al. 2003). The jacking force of each tendon was 0.60 MN (135 kip) (DRC 1996). There were 316 tendons above the main pier, densely packed in four layers within the top slab (see Fig. 2). Their combined initial prestressing force was approximately 190 MN (42,606 kip) (Yee 1979; Pilz 1997; McDonald et al. 2003). The same threaded bars were used to provide vertical prestress in the webs and horizontal transverse prestress in the top slab. The tendon spacing in the webs ranged from 0.3 to 3 m (1 to 10 ft) (Khaled Shawwaf, personal communication, September, 18, 2008). The horizontal transverse tendons in the top slab were spaced at 0.56 m (22 in.) (ABAM 1993; McDonald et al. 2003).

The alloy steel of the tendons had a yield strength of 1,034 MPa (150 ksi) and an ultimate strength of 1,054 MPa (153 ksi) (DRC 1996). Its Young's elastic modulus was assumed to be 200 GPa (29,000 ksi), and the Poisson's ratio was assumed to be 0.3. Unprestressed steel reinforcement (ABAM 1993) was taken into account in the calculations. In postcollapse examination, neither the prestressed nor the unprestressed steel showed any signs of significant corrosion despite the tropical marine environment, although some of the ducts showed mild corrosion.

The construction of each segment took slightly more than one week (TYLI 1996). When the concrete strength in the segment just cast attained 17.2 MPa (2,500 psi), 6–12 tendons were stressed to 50% of their final jacking force (TYLI 1996). When the concrete strength reached 24.1 MPa (3,500 psi), all the tendons terminating in this segment were stressed fully. The segmental erection of the opposite symmetric cantilevers was almost simultaneous and took 6–7 months (Yee 1979).

Although the construction was closely monitored, the camber that was planned to offset the anticipated long-term deflections was not met. The creep and shrinkage during the segmental erection caused an unintentional initial sag of 229 mm (9 in.) at midspan that could not be corrected during the erection because it would have required abrupt large changes of slope (Khaled Shawwaf, personal communication, September 18, 2008). The initial sag before installation of the midspan hinge was not included in the reported deflection measurements or in the deflection curves in the figures.

The initial deflections for the first 2 years were benign. However, in 1990, the longer-term deflections revealed that the midspan deflection had reached 1.22 m (48 in.) (JICA 1990), which caused ride discomfort, vibrations after vehicle passage, and excessive deterioration of the road surface. By 1993 (ABAM 1993), the deflection had reached 1.32 m (52 in.). In 1995, just before removal of the roadway pavement [average thickness of 76 mm (3 in.)], the midspan deflection had reached 1.39 m (54.7 in.) and was still growing (Berger/ABAM 1995a).

Creep and Shrinkage Models Considered

As an adequate approximation under service conditions, concrete can be assumed to follow aging linear viscoelasticity with corrections for tensile cracking, variations of humidity and temperature, and drying creep (or the Pickett effect). The concrete deformation is then fully characterized by one of the existing prediction models for the shrinkage strain $\epsilon_{sh}(t)$ and the compliance function $J(t, t')$. The prediction models considered in the analysis were the ACI model (ACI 1971, 2008a), the Comité Euro-Internationale du Béton (CEB), Fédération internationale de la précontrainte (FIP) (or

CEB-FIP, or fib) model (Fédération internationale du béton, fib 1999), the Japan Society of Civil Engineers (JSCE) model (JSCE 1991), the Gardner and Lockman (GL) model (Gardner 2000; Gardner and Lockman 2001), and Model B3 (Bažant and Baweja 1995, 2000; Bažant and Prasanna 1988, 1989a, b; Jirásek and Bažant 2002). The same computer program, ABAQUS (SIMULIA, Providence, Rhode Island), with the same step-by-step time integration based on the Kelvin chain, was used for all models (see Bažant et al. 2012).

The smallest deviations from the data were obtained with Model B3 based on the solidification theory (Bažant and Prasanna 1989a, b), which was first presented in 1995 (Bažant and Baweja 1995), slightly updated in 2000 (Bažant and Baweja 2000), and summarized in Jirásek and Bažant (2002). Model B3 represents a refinement of the earlier Bažant-Panula and Bažant-Panula-Kim-Xi models (Bažant and Panula 1978a, b, c, d, 1979a, b; Bažant and Kim 1991b, 1992a, b, c; Bažant et al. 1991, 1992). The theoretical justification has been provided in several studies (Bažant et al. 1997; Bažant 2000, 2001). The form of the B3 compliance function for basic creep was theoretically derived and experimentally supported in Bažant and Prasanna (1988, 1989a, b). In statistically unbiased comparisons with a large database (Bažant and Li 2008a), Model B3 was clearly superior to the other existing models (Bažant and Li 2008b; Bažant et al. 2008).

The input parameters of the creep and shrinkage prediction models are divided into extrinsic and intrinsic. For all models, the extrinsic parameters, which include the environmental factors, are the following:

1. The age at the start of drying, taken here as $t_c = 7$ days, which is the mean period of the segmental erection cycle ranging from 5 to 10 days (Khaled Shawwaf, personal communication, September 18, 2008; TYLI 1996);
2. The average environmental humidity $h = 0.70$;
3. The effective thickness of cross section $D = 2 V/S$, in which a minor correction k_s for body shape is applied in the case of Model B3; $k_s = 1$ for all slabs and webs considered here ($V/S = \text{volume—surface ratio}$); and
4. For the extended Model B3 only, and also the temperature.

The intrinsic input parameters, which reflect the composition of concrete, vary from model to model. Formulation of the ACI, CEB, and GL models was driven by the desire for simplicity. Accordingly, the only important intrinsic parameter in these models is the standard 28-day compression strength f'_c , while other major influencing parameters such as the cement content and the water-cement and aggregate-cement ratios are not taken into account.

Model B3 is special in that the free intrinsic input parameters are more than one. They introduce the main aspects of concrete composition. If unknown, they can be set equal to their recommended default values. Their advantages are that reasonable ranges of the unknown concrete mix parameters can be explored, computation of structural responses for various plausible sets of values of these parameters can be run, and a picture of the possible range of structural responses to expect can be obtained. Two sets of input parameters have been considered in the computations.

Set 1 Pure Prediction

The mean 28-day compressive strength f'_{cr} of concrete was approximately 35.9 MPa (5,200 psi), as indicated by the cylinder tests during construction reported by Raymond Zelinski (personal communication, December 12, 2010). However, in Bažant et al. (2010), the value of 35.9 MPa was considered according to ABAM (1993) to be the 28-day specified compressive strength f'_c . The mean strength \bar{f}_c from the cylinder tests during construction must not have been lower than f'_{cr} ; and according to the ACI code

(ACI 2008b), Zelinski's value implies that $f'_c \leq 35.9 \text{ MPa} - \Delta f$, where $\Delta f \approx 1.34 \times \text{standard deviation}$ (Bažant and Yu 2006), which would have been much less than 35.9 MPa. On the other hand, the f'_c value from ABAM (1993) implies that $f'_{cr} \approx 35.9 \text{ MPa} + \Delta f$. ABAM and Zelinski cannot both be right. The records of Zelinski (the resident engineer at the KB Bridge construction representing both the designer, Alfred A. Yee & Associates, and the owner, the Trust Territory Government) are deemed more reliable, and so the curves from Bažant et al. (2010) had to be recalculated. Nonetheless, the recalculation changed the results very little because other Zelinski's input changes happened to compensate. Furthermore, the prediction models should properly use the mean strength or an estimated f'_{cr} , as stated in Model B3, but the ACI Guide (ACI 2008a) specifies the use of f'_c for all models. To keep the results comparable, f'_c had to be used as the input for all models, including B3 Set 1.

The 28-day elastic modulus E_c was neither specified in design nor measured on the site. The modulus value was measured on core samples just before the retrofit, but this value is appropriate for Set 2 and must not be used for Set 1, which is intended to check the prediction capability. The only way that E_c could be estimated at the time of design was from the approximate ACI formula $E_c = (57,000 \text{ psi}) \sqrt{f'_{cr}(\text{psi})}$, which gives $E_c = 28.3 \text{ GPa}$ (4,110 ksi). Furthermore, according to Zelinski's records, the specific cement content c was 535 kg/m^3 (33.4 lb/ft³), the aggregate-cement ratio a/c was 2.90, and the water-cement ratio w/c was 0.40 (in which a superplasticizer was used). A higher w/c value was considered in Bažant et al. (2010), but this was an estimate from ABAM (1993) and Khaled Shawwaf (personal communication, September 18, 2008).

On the basis of the foregoing input, the B3 empirical formulas (Bažant and Baweja 2000) yield the following Model B3 parameters, which are different from Bažant et al. (2010):

$$q_1 = 0.146, \quad q_2 = 1.42, \quad q_3 = 0.011, \quad q_4 = 0.080, \\ q_5 = 2.33(\times 10^{-6}/\text{psi}) \quad (1)$$

$$\varepsilon_{k\infty} = 0.000981 \quad \text{and} \quad k_t = 19.2 \quad (\text{set 1}) \quad (2)$$

where the values of q_2 , q_3 , and q_4 are increased by 20% because of the mean of the plasticizer effects observed by Brooks (2000) (the use of plasticizer was not known in Bažant et al. 2010).

Set 2 Updated

For a better estimate, only the values of q_2 , q_5 , and $\varepsilon_{s\infty}$, governing mainly the response for the first few years, have been estimated from the composition, and the estimates of the remaining parameters were improved as follows:

$$q_1 = 0.188, \quad q_3 = 0.262, \quad q_4 = 0.140(\times 10^{-6}/\text{psi}) \\ (\text{as changed for set 2}) \quad (3)$$

where q_1 was adjusted according to the elastic modulus obtained in the truck load test (Bažant et al. 2010). Here, q_3 and q_4 were identified by a trial-and-error procedure, conducted with two objectives in mind: (1) stay close to the values of multidecade creep tests, which are only the 30-year tests of Brooks (1984, 2005); and (2) obtain the closest possible fit of the measured deflection of the KB Bridge. Fig. 3 indicates that the selected intrinsic parameters agree with these tests reasonably well.

It has been noted that the compliance function $J(t, t')$ agrees with the 30-year tests of Brooks and is in good agreement with

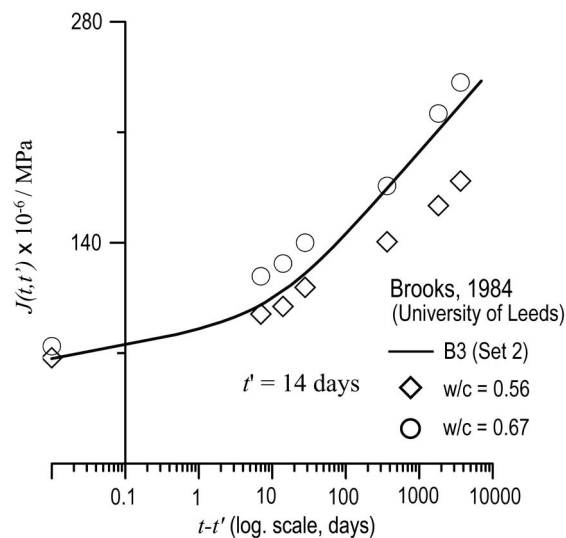


Fig. 3. Model B3 curve for adjusted q_3 and q_4 compared with the creep tests by Brooks (1984, 2005)

the measured deflections. This result suggests using these tests for recalibrating input parameters q_3 and q_4 , which are the main controlling parameters of the multidecade creep in Model B3 and are difficult to estimate from the database because the database is dominated by test data for load durations < 5 years.

To calculate and compare the predictions of various models, all the properties of the concrete and the environmental histories of the KB Bridge concrete would have to be known, but they are not. Therefore, comparing the predictions of various models either mutually or with the observations is not fully informative. Nevertheless, what can be compared is whether the observed deflections are within the realistic range of each model. They are indeed within the realistic range for Model B3 but not at all for other models, including the ACI, CEB, JSCE, and GL models.

For Model B3, the predictions are not fixed because there exist input parameters that are uncertain for the KB Bridge and are thus free to be set within their realistic range. The predictions of the other models are fixed by the reported value of the concrete strength, with no flexibility of adjustment (a partial exception is the JSCE model, which takes into account the water content w and cement content c). The data available for the KB Bridge, as presented here, do not suffice to obtain a unique compliance function for this bridge unless the default parameter values are used; they do suffice to obtain unique compliance functions for the ACI, CEB, JSCE, and GL models—although at the cost of ignoring many important influences.

Some engineers want the model to predict the creep and shrinkage from as few parameters as possible, particularly from the concrete design strength only (ACI 2008a). This might be more convenient, but it is not realistic. If the additional parameters of Model B3 for a given concrete are known, better predictions can be made. If they are unknown, they can be assigned their typical, or default, values, and thus predictions can still be made even if only the strength is known. Furthermore, by varying the influencing parameters of Model B3 through their realistic range, a realistic range of expected responses can be explored; and a structure for the most unfavorable realistic combination can be designed. With the other models, one can explore only the effect of strength variation.

Computed Deflections, Prestress Loss, and Comparisons to Measurements

Because of symmetry, only one-half of the bridge was analyzed. A three-dimensional (3D) finite-element program that automatically captured all the stress-redistribution effects attributable to creep was used (see the mesh in Fig. 2). As a first check of the program, a comparison was made with the bridge stiffness, which was measured in January 1990 in a load test by JICA (1990). An average downward deflection of 30.5 mm (0.10 ft) was recorded at midspan when two 12.5 t trucks were parked side by side on each side of the midspan hinge (a previous paper erroneously assumed that only one truck was parked on each side). The front wheels of the

two trucks on each side were assumed to have been 3 m away from the midspan. The rear wheels, 12 m behind the front wheels, were assumed to carry 60% of the truck weight. The finite-element code predicted the deflection of 30 mm (0.098 ft) that was measured approximately within 2.4 h (the 2.4 h creep was based on Model B3 Set 2) under a load of 245 kN (55.1 kip). Given the uncertainty about the actual rate of loading, the difference was small enough.

The results of the calculations are shown in Figs. 4–7, both in linear and logarithmic time scales ($t - t_1$ = time measured from the end of construction; t_1 = time when the midspan hinge was installed). The data points show the measured values. The circles represent the data reported by the firm that investigated the excessive deflections (JICA 1990), and the diamonds represent the data

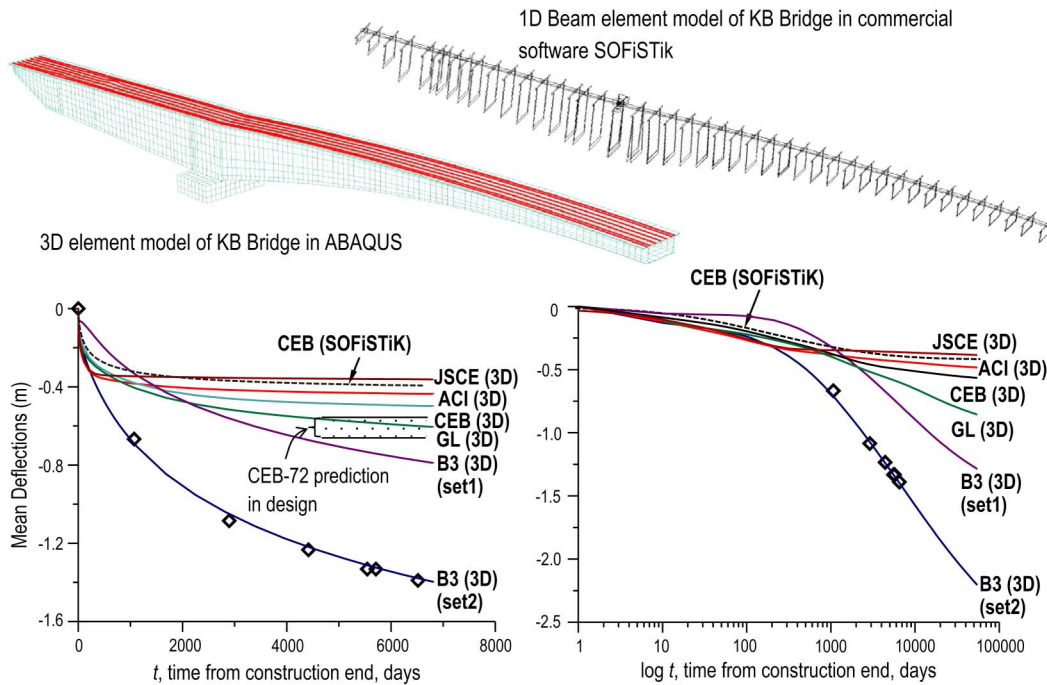


Fig. 4. Mean deflections calculated using Model B3 and the ACI, CEB (one using SOFiSTiK), JSCE, and GL models in normal and logarithmic scales

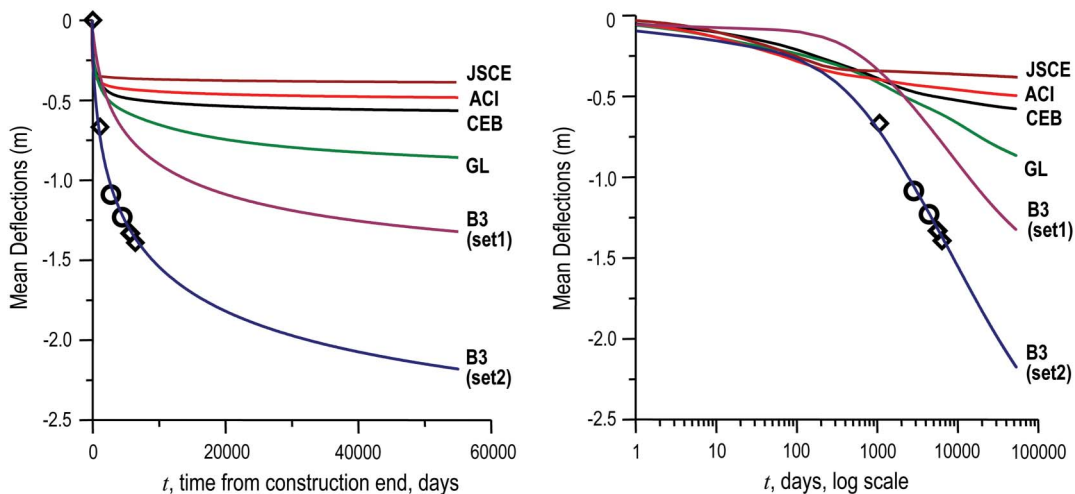


Fig. 5. Mean deflections calculated as in Fig. 4 but for time extended up to 150 years (assuming no retrofit and no collapse have taken place)

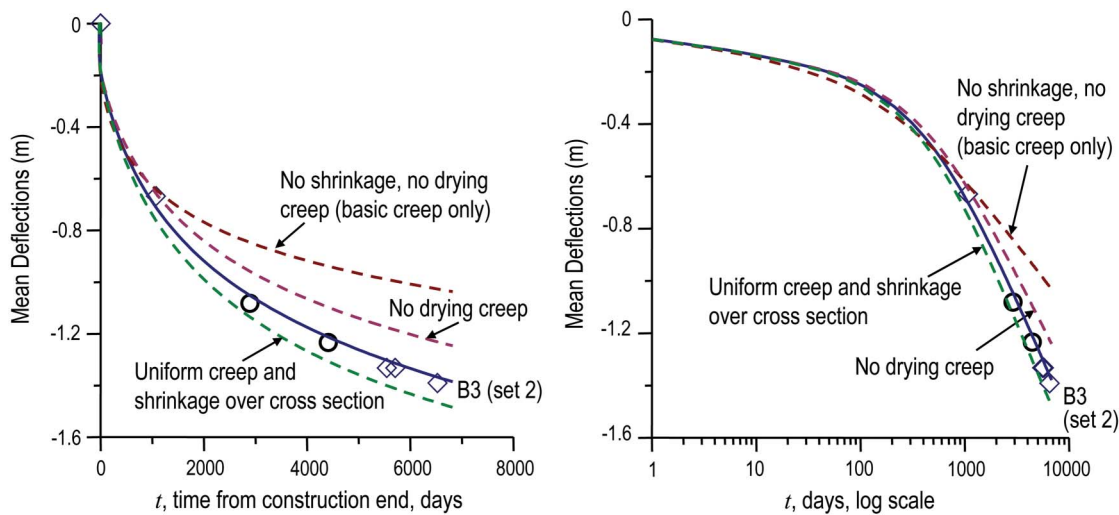


Fig. 6. Deflections in normal and logarithmic scales computed using Model B3 for (1) no drying creep; (2) no shrinkage and no drying creep; (3) uniform creep and shrinkage over the cross section

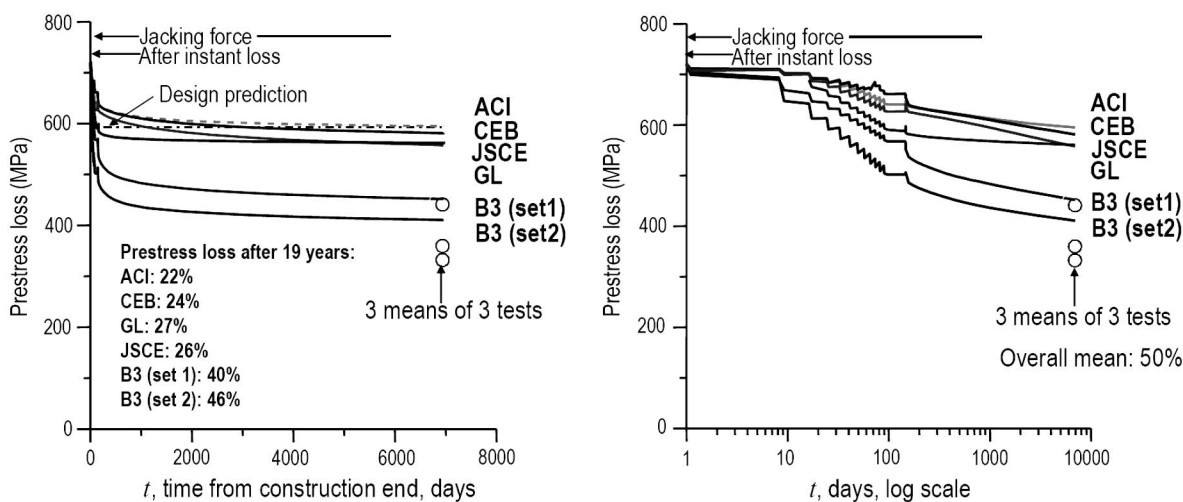


Fig. 7. Prestress loss in tendons at the main pier using Model B3 and the ACI, CEB, JSCE, and GL models in normal and logarithmic scales

accepted from a secondary source (Berger/ABAM 1995a). For comparison, Figs. 4–7 show the results obtained with Model B3 and the ACI, CEB, JSCE, and GL models. All these responses were computed with the same finite-element program and the same step-by-step time integration algorithm. For Model B3, it was possible to consider the effect of the differences in thickness of the slabs and webs on their drying rates. In Fig. 4, the deflection obtained by using the popular commercial program SOFiStiK, which is based on the one-dimensional beam element model, is also demonstrated (Yu et al. 2012).

Fig. 4 shows the calculated deflection curves up to the moment of retrofit at approximately 19 years of age. Except for the curves in the JSCE model, the curves differ only slightly from those in Bažant et al. (2010) because of the input being compensated by various changes. Because a lifetime well beyond 100 years is generally expected, Fig. 5 shows the same curves extended up to 150 years under the assumption that there has been no retrofit and, thus, no collapse.

Fig. 6 presents the midspan deflection that is obtained (1) if the drying creep is neglected, (2) if both the shrinkage and drying creep are neglected, and (3) if the shrinkage and the drying creep compliance are considered to be uniform over the cross section and to be deduced from the overall effective thickness $D = 2V/S$ of the whole cross section. The use of uniform creep and shrinkage properties throughout the cross section neglects the curvature growth attributable to differential shrinkage and differential drying creep and gives results dominated by the unusually thin webs. Also, the effect of mean drying can be very different from the mean of the effects of drying in the individual slabs (Bažant et al. 1992).

The shear lag effect with the associated creep-induced stress redistributions within the cross sections necessitates 3D simulations. It cannot be realistically captured by the classical concept of effective width of the top slab (which was actually used in the design of the KB Bridge). The computations show that the shear lag occurs in four different ways—in the transmission of vertical shear force because of the vertical reaction at the pier, in the transmission of

the concentrated forces from tendon anchors, and for each of these in the horizontal slabs and in the vertical walls. Only full 3D analysis can capture this behavior. It always yields larger deflections and larger prestress losses. For the bridge in Palau, the beam-type analysis causes an error of -20% in deflections and -10% in the prestress loss. The errors are larger in the 95% confidence limits, discussed subsequently.

Accuracy in calculating the prestress loss is crucial because the bridge deflection is a small difference of two large, but uncertain, numbers—the downward deflection because of self-weight and the upward deflection because of prestress. Calculations show that, compared with the classical theory of bending, all the shear lags combined increased the elastic downward deflection by 18% because of self-weight and the elastic upward deflection by 14% because of initial prestress, which jointly produced the aforementioned total shear lag effect of 20%.

Steel relaxation is a viscoplastic phenomenon (Jirásek and Bažant 2002) that occurs at variable, rather than constant, strain and is strongly influenced by elevated temperature, as described by the viscoplastic constitutive law given in Part II, Bažant et al. (2012) (see Bažant and Yu 2011). That law builds on the formulas for constant strain relaxation used in both the European code (CEB-FIP 1990; FIB 2010) and American practice (Magura et al. 1964; Nawy 2006), formulates the strain change effects as validated by the experiments of Buckler and Scribner (1985), and introduces the temperature effect through the activation energy and the Arrhenius factor (Cottrell 1964) calibrated by the data from fib (2010, see Figs. 5.3–5.5 therein). The calculations in Part II (Bažant et al. 2012) showed that the heating of the top slab by the tropical sun must have significantly intensified the steel stress relaxation, which in turn must have increased the deflections.

The simulation of the bridge in Palau indicated that the excessive deflection was accompanied by the longitudinal creep and shrinkage contraction of the box girder. Although this contraction tended to cause a reduction of the subsequent prestress loss, the temperature increase because of solar heating of the top slab together with the continuing longitudinal creep and shrinkage contraction of the concrete more than compensated for this reduction. This caused the excessive prestress loss to continue and eventually reach values much higher than those for the constant strain of the steel and constant temperature.

The environmental fluctuations of both temperature and humidity also affect the concrete, while heating of the top slab by the tropical sun significantly increased the relaxation of the embedded tendons and, thus, also the deflections of the bridge (see Bažant et al. 2012), the daily temperature fluctuations have little overall effect on the concrete, and seasonal temperatures are negligible in the tropics. Even at higher latitudes, the humidity fluctuations because of the weather and the seasonal changes are not too important for multidecade deflections because the moisture diffusivity is approximately 1,000 times lower than the thermal diffusivity (Bažant et al. 2003). This fact is documented by the smoothness of the measured deflection histories of 55 bridges presented in Bažant et al. (2011a, b, c).

The measured deflection at 18 years after span closing, which was 1.39 m, closely matched the deflection calculated from Model B3 with Set 2 parameters. This measured deflection was roughly three times larger than that calculated for the ACI or CEB model (which was 0.47 m or 0.53 m), and approximately double the measured deflection calculated for the GL model (which was 0.65 m) (see Fig. 4). The ACI, CEB, JSCE, and GL deflection curves had shapes that were rather different from those of Model B3 as well as those of the observed deflection history. They all gave far too much deflection growth during the first year and far too little from

three years on, especially for the ACI, CEB, and JSCE models. The 19-year prestress loss was only 22% and 24% when the ACI and CEB models were used in the present finite-element code but approximately 46% when Model B3 was used (see Fig. 7) (again, the changes from Bažant et al. 2010 are only slight).

The correctness of the prestress loss predicted by Model B3 was confirmed by the stress relief tests that were made by ABAM on three tendons just before the retrofit (Berger/ABAM 1995a). Sections of three tendons were bared, and strain gauges were glued at three different locations on each of the three tendons. Each of these tendons was then cut, and the stress was calculated from the shortening measured by the gauge next to the cut (see Table 1). The average stress obtained from nine measurements on the tendons was 377 MPa (54.7 ksi), indicating that the average prestress loss over 19 years was approximately 50%. The coefficient of variation was 12.3%. Model B3 (Set 2) calculations gave a prestress loss of 46%, which deviated from the measured mean by only 9%. This was less than the coefficient of variation of these measurements, which was 12.3%. Similar tests were also conducted by another investigating company (Wiss, Janey and Elstner, Highland Park, Illinois), and the average measured prestress loss was almost same.

Only nondestructive methods are normally permitted. This makes it next to impossible to measure the stresses in grouted tendons; however, for the KB Bridge, the cutting of tendons was not a major sacrifice because additional tendons were to be installed anyway. Thus, the decision to retrofit furnished a unique opportunity to learn about the actual prestress losses.

In the mid-1970s, the prestress loss was calculated not by finite elements but by simple formulas based on the beam theory (e.g., Nilson 1987). A lump estimate of the final prestress loss was generally used; and according to Khaled Shawwaf (personal communication, September, 18, 2008), it was used for the KB Bridge. According to the lump estimate, the prestress loss would have been 22%, which is marked in Fig. 7 by a horizontal dashed line. Compared with the measurements, the errors of this estimate are enormous, and so are the errors compared with the present calculation based on Model B3. These errors are one reason that the long-term deflections were so badly underestimated in design. For large box girders, the standard textbook formulas for prestress loss are inadequate and dangerously misleading.

According to the ACI, CEB, and the JSCE models, the compliance curves and the deflection curves terminate with a horizontal asymptote. However, according to Model B3, the long-term compliance curves are logarithmic. Thus, Model B3 predicts that the

Table 1. Summary of Strain Relief Tests of Prestressed Tendons of the KB Bridge in Palau (Berger/ABAM 1995a)

Tendon	Location	Δ_1 ($\mu\epsilon$)	Δ_2 ($\mu\epsilon$)	Δ_3 ($\mu\epsilon$)	Mean Δ ($\mu\epsilon$)	σ (MPa)
1	1	1,640	1,640	1,630	1,637	327.3
	2	1,650	1,640	1,650	1,647	329.3
	3	1,680	1,700	1,710	1,697	339.3
	Average					332.0
2	4	1,810	1,820	1,790	1,807	361.3
	5	1,810	1,800	1,790	1,800	360.0
	6	1,780	1,790	1,790	1,787	357.3
	Average					359.6
3	7	2,250	2,230	2,220	2,233	446.7
	8	2,220	2,220	2,210	2,217	443.3
	9	2,170	2,150	2,170	2,163	432.7
	Average					440.9

deflection curve terminates in the logarithmic time scale with an asymptote that is a straight line of a finite slope, which agrees very well with the observations (Fig. 4). However, the final slope predicted by Model B3 (Set 1) for 18 years is too small. To match the slope in Fig. 4, it would need to be increased by a factor of 1.52.

For times longer than approximately three years, the deflections were observed to evolve almost linearly in the logarithmic time scale, an outcome that is to be expected for theoretical reasons (Bažant 2000) and can thus be extrapolated to longer times graphically (see Fig. 5). The graphical straight-line extrapolation is observed to agree almost exactly with the Model B3 calculations up to 150 years. It is virtually certain that if the bridge were left standing without any retrofit, the 150-year deflection would have reached 2.24 m (7.35 ft), well beyond the limit of serviceability.

Capturing the initial deflection history correctly is essential for correct extrapolation in order to predict subsequent problems. The differential shrinkage and drying creep due to nonuniform drying is important in this respect (Křístek et al. 2005, 2006, 2008). In Fig. 4, Model B3 gives by far the closest prediction for the early deflection history.

Excessive Long-Term Deflections of Other Box Girders

It is deplorable that the data on excessive deflections usually go unpublished. Nevertheless, Y. Watanabe, the chief engineer of Shimizu Corp., Tokyo, graciously made available the data on some large Japanese bridges that epitomize the experience in many

other countries. These deflection data are plotted in Fig. 8, in which the data points represent the measured deflections and the dashed curves show the prediction based on the design recommendations of the Japan Road Association (JRA). The solid curves give the predictions of Model B3 calculated in the same way as for the KB Bridge after adjusting the composition parameters similarly to Set 2.

The foregoing observations document that the deflections of the KB Bridge are not a unique occurrence. Interestingly, one of these four bridges, Urado, did not show excessive 30-year deflection; the reason may be that the creep curve in the JRA code was set approximately 60% higher than in the JSCE code. However, the deflection slope at 30 years portends future problems.

The absence of a midspan hinge has been known to reduce deflections. However, it is not a panacea. Even bridges without a midspan hinge, designed by the code, can suffer excessive deflections. This outcome, for example, is documented by the data on the Děčín Bridge over the Labe in North Bohemia (see Fig. 9).

Model B3 Improvement and Need for Inverse Analysis of Many Bridges

Based on the parameter values obtained for Set 2 and on the comparisons with deflection measurements, it has been determined that the multidecade deflection prediction could be improved by replacing the B3 formulas (Bažant and Baweja 1995, 2000) for q_3 and q_4 with the following:

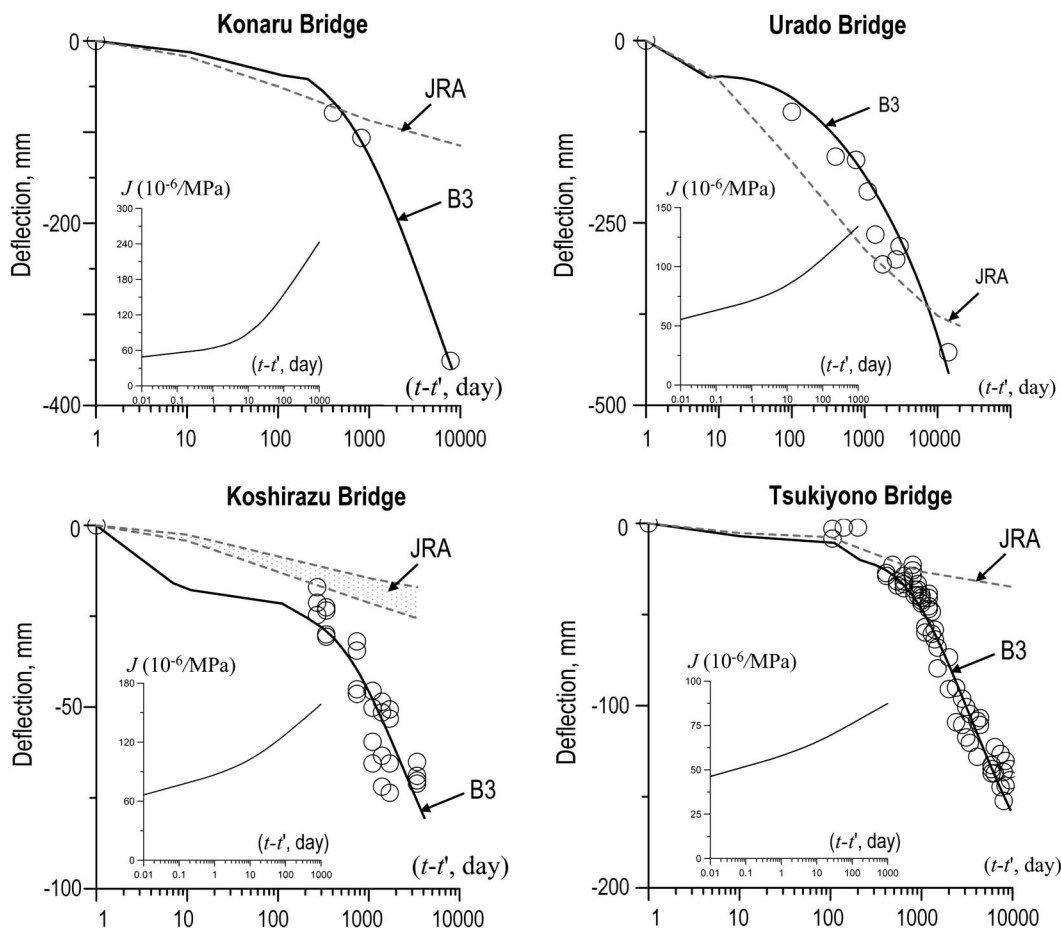


Fig. 8. Excessive deflections observed in four Japanese bridges

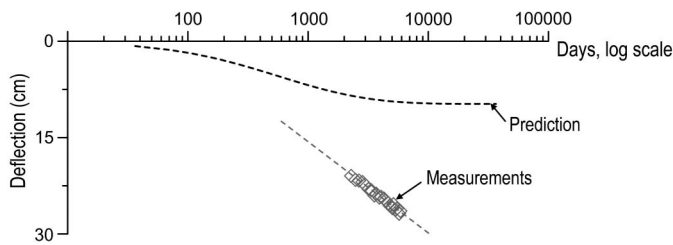


Fig. 9. Excessive deflections observed in a continuous bridge in the Czech Republic (images courtesy Lukas Vrablik, with permission)

$$q_3 = (w/c)^2 q_2, \quad q_4 = 0.3(a/c)^{-0.7} \quad (4)$$

in which w/c and a/c = water-cement and aggregate-cement ratios by weight, respectively. However, the data on one or several bridges do not suffice to overcome the extreme scarcity of multidecade test data (Bažant and Li 2008a). For optimal recalibration of the B3 prediction of material parameters from concrete composition and strength, it will be necessary to gather data on the deflections of many box girder bridges and then conduct inverse finite-element creep analysis with optimization.

Uncertainty of Deflection Predictions and Calculation of Confidence Limits

Creep and shrinkage are notorious for their relatively high random scatter. For this reason, it has previously been argued (Bažant and Kim 1989, 1991) that the design should be made not for the mean deflections but for some suitable confidence limits such as 95% (Bažant and Liu 1985; Bažant et al. 2010). By adopting Latin hypercube sampling of the input parameters (Bažant and Liu 1985; Bažant and Kim 1989), such confidence limits can easily

be obtained by repeating the deterministic computer analysis of a bridge according to Model B3 eight times—one run for each of eight different randomly generated samples of eight input parameters.

The range of the cumulative distribution of each random input variable (assumed to be Gaussian) is partitioned into N intervals of equal probability. The parameter values corresponding to the centroids of these intervals are selected according to randomly generated Latin hypercube tables (these tables can be freely downloaded from the ITI website, <http://iti.northwestern.edu/generator>, so a bridge designer would not need to work with a random number generator). The values from the rows of these tables are then used as the input parameters for N deterministic computer runs of creep and shrinkage analysis.

Choose $N = n$ = number of random input parameters (here, $N = n = 8$) is sufficient. One random input variable is the environmental relative humidity h , with the mean and coefficient of variation being estimated as 0.70 and 0.2 (70% and 20%). The other parameters are the material characteristics $q_1, q_2, q_3, q_4, q_5, k_t$, and ε_∞ , representing the parameters of Model B3. According to Model B3, the means of these parameters for the KB Bridge were assumed to be $q_1 = 0.188, q_2 = 1.42, q_3 = 0.262, q_4 = 0.14, q_5 = 2.33, k_t = 19.2$, and $\varepsilon_\infty = 0.000981$. The estimated coefficient of variation was 23% for creep parameters q_1, q_2 , and q_5 , and 30% for q_3 and q_4 (these have a higher uncertainty as they relate to long-term creep and data relating to this are scarce). For shrinkage parameters k_t and ε_∞ (Bažant and Panula 1978a, b, c, d; Bažant and Baweja 1995, 2000), the estimated coefficient of variation was 34%.

The responses from each deterministic computer run for Model B3 (Set 2), particularly the midspan deflections at specified times, were collected in one histogram of eight values, with the mean \bar{w} and coefficient of variation ω_w being the desired statistics. Knowing these and assuming the Gaussian (or normal) distribution, the one-sided 95% confidence limit was obtained as $w_{95} = \bar{w}(1 + 1.645 \omega_w)$ (i.e., the limit that was exceeded with a probability of 5%). In other words, the limit would be exceeded by one out of 20 identical bridges, which seems to give the optimal balance between risk and cost.

The curves of the mean and the one-sided 95% and 5% confidence limits for the KB Bridge in Palau are shown for Model B3,

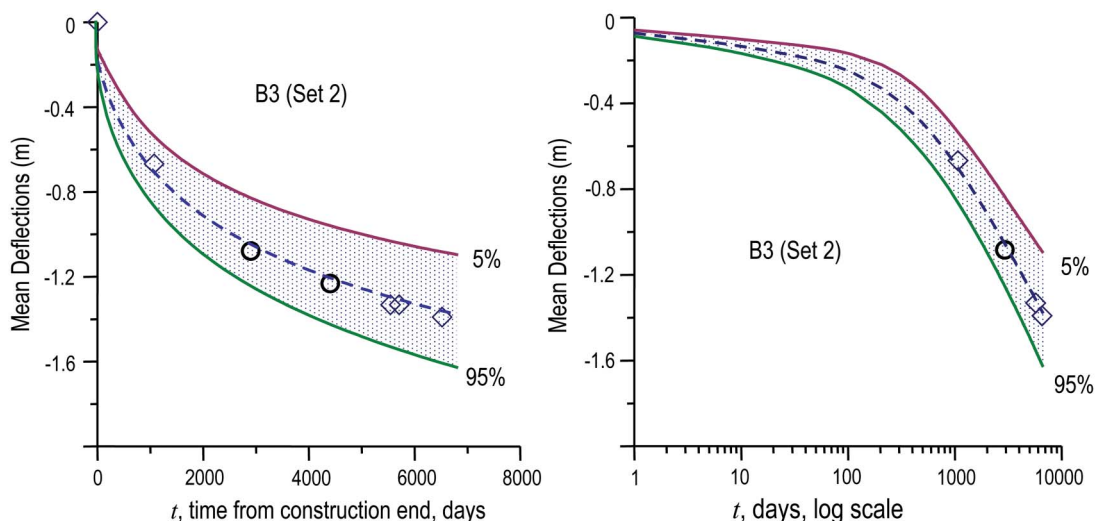


Fig. 10. Mean response and 95% confidence limits of Model B3 in normal and logarithmic scales

Set 2, in Fig. 10. The curves of the present finite-element calculations according to the ACI and CEB models lie way outside the statistical confidence band obtained with Model B3, and the traditional prediction lies even farther outside the confidence band.

Using the database (Bažant and Li 2008a) as the prior information, the statistics of long-term deflection can be further improved by means of Bayesian statistical analysis (Křístek and Bažant 1987). The probabilistic problem of deflections is fortunately much easier than the problem of structural safety. For the latter, the extreme value statistical theory must be used, because the tolerable probability of failure is $< 10^{-6}$, far less than the value of 0.05 that is acceptable for deflections.

Summary of the Main Causes of Underestimation of Deflections and Prestress Loss

In the order of decreasing importance, the main causes of underestimation of deflections and prestress loss are as follows:

1. Poor material model for creep and shrinkage;
2. Beam-type analysis instead of a full 3D analysis;
3. Differences in the rates of shrinkage and drying creep because of different thicknesses of slabs in the box cross section; and
4. Lack of statistical estimation of the range of possible responses.

Detailed conclusions will be presented in Part II (Bažant et al. 2012).

Appendix. Resolution of Third Structural Engineers World Congress

1. The structural engineers gathered at their Third World Congress deplore the fact the technical data on the collapses of various large structures, including the Koror-Babeldaob Bridge in Palau, have been sealed as a result of legal litigation.
2. They believe that the release of all such data would likely lead to progress in structural engineering and possibly prevent further collapses of large concrete structures.
3. In the name of engineering ethics, they call for the immediate release of all such data. [Proposed at the congress by Z. P. Bažant, in the name of the following group of experts whose support has been obtained in advance: C. Andrade (Madrid), L. Belarbi (Missouri), N. Bičanić (Glasgow), I. Carol (Barcelona), L. Cedolin (Politecnico di Milano), T.-P. Chang (Taipei), J.-C. Chern (Taipei), W. Dilger (University of Calgary), L. Elfgren (Lulea), R. Eligehausen (Stuttgart University), E. Fairbairn (Rio de Janeiro), D. M. Frangopol (Lehigh), P. Gambarova (Politecnico di Milano), W. Gerstle (University of New Mexico), N. M. Hawkins (Seattle), A. Ingrassia (Cornell University), M. Jirásek (CTU Prague), J. W. Ju (Los Angeles), M. T. Kazemi (Tehran), J.-K. Kim (KAUST, Korea), V. Křístek (CTU Prague), C. Leung (HKUST, Hong Kong), Z.-J. Li (Hong-Kong), K. Maekawa (University of Tokyo), G. Maier (Politecnico di Milano), C. Majorana (University of Padua), H. Mang (Vienna), P. Marti (ETHZ), H. Mhashi (Sendai), D. Novák (BTU Brno), J. Ožbolt (Stuttgart University), B. Raghun-Prasad (Bangalore), I. Robertson (Honolulu), J. G. Rots (Delft), V. Saouma (Boulder), B. Schrefler (Padua), Susanto Teng (Singapore), S. Teng (Singapore), T. Tanabe (Nagoya), T. Tsubaki (Yokohama), F.-J. Ulm (MIT), J. van Mier (ETHZ), C. Videla (Santiago), M. Vořechovský (BTU Brno), K. Willam (University of Colorado at Boulder), Y. Xi (Boulder), and A. Zingoni (Cape Town)].

References

- ABAM Engineers Inc. (ABAM). (1993). "Koror-Babeldaob bridge repairs: Basis for design." *Bureau of Public Works Rep.*, ABAM, Koror, Republic of Palau.
- American Concrete Institute (ACI). (1971). "Prediction of creep, shrinkage and temperature effects in concrete structures." *Designing for effects of creep, shrinkage and temperature in concrete structures*, ACI, Detroit, 51–93.
- American Concrete Institute Committee 209 (ACI). (2008a). "Guide for modeling and calculating shrinkage and creep in hardened concrete." *ACI Rep. 209.2R-08*, ACI, Farmington Hills, MI.
- American Concrete Institute Committee 318 (ACI). (2008b). *Building code requirements for structural concrete (ACI 318-05) and commentary (ACI 318-05)*, ACI, Farmington Hills, MI.
- Bažant, Z. P. (2000). "Criteria for rational prediction of creep and shrinkage of concrete." *Adam Neville symposium: Creep and shrinkage—structural design effects*, A. Al-Manaseer, ed., ACI, Farmington Hills, MI, 237–260.
- Bažant, Z. P. (2001). "Creep of concrete." *Encyclopedia of materials: Science and technology*, K. H. J. Buschow et al., ed., Vol. 2C, Elsevier, Amsterdam, Netherlands, 1797–1800.
- Bažant, Z. P., and Baweja, S. (1995). "Creep and shrinkage prediction model for analysis and design of concrete structures: Model B3." *Mater. Struct.*, 28(6), 357–367.
- Bažant, Z. P., and Baweja, S. (2000). "Creep and shrinkage prediction model for analysis and design of concrete structures: Model B3." *The Adam Neville symposium: Creep and shrinkage—Structural design effects*, A. Al-Manaseer, ed., ACI, Farmington Hills, MI, 1–83.
- Bažant, Z. P., Hauggaard, A. B., Baweja, S., and Ulm, F.-J. (1997). "Microprestressing-solidification theory for concrete creep. I. Aging and drying effects." *J. Eng. Mech.*, 123(11), 1188–1194.
- Bažant, Z. P., Hubler, M. H., and Yu, Q. (2011a). "Pervasiveness of excessive segmental bridge deflections: Wake-up call for creep." *ACI Struct. J.*, 108(6), 766–774.
- Bažant, Z. P., Hubler, M. H., and Yu, Q. (2011b). "Ubiquity of excessive multi-decade segmental bridge deflections: A revelation." *ACI Concrete International Rep.*, Northwestern Univ., Evanston, IL.
- Bažant, Z. P., Hubler, M. H., Yu, Q., Křístek, V., and Bittnar, Z. (2011c). "Wake-up call for creep, myth about size effect and black holes in safety." *Proc., fib Congress*, Prague, Czech Republic.
- Bažant, Z. P., and Kim, J.-K. (1989). "Segmental box girder: Deflection probability and Bayesian updating." *J. Struct. Eng.*, 115(10), 2528–2547.
- Bažant, Z. P., and Kim, J.-K. (1991a). "Segmental box girder: Effect of spatial random variability of material on deflections." *J. Struct. Eng.*, 117(8), 2542–2547.
- Bažant, Z. P., and Kim, J.-K. (1991b). "Improved prediction model for time-dependent deformations of concrete: Part 2—Basic creep." *Mater. Struct.*, 24(6), 409–421.
- Bažant, Z. P., and Kim, J.-K. (1992a). "Improved prediction model for time-dependent deformations of concrete: Part 3—Creep at drying." *Mater. Struct.*, 25(1), 21–28.
- Bažant, Z. P., and Kim, J.-K. (1992b). "Improved prediction model for time-dependent deformations of concrete: Part 4—Temperature effects." *Mater. Struct.*, 25(2), 84–94.
- Bažant, Z. P., and Kim, J.-K. (1992c). "Improved prediction model for time-dependent deformations of concrete: Part 5—Cyclic load and cyclic humidity." *Mater. Struct.*, 25(3), 163–169.
- Bažant, Z. P., Kim, J.-K., and Jeon, S.-E. (2003). "Cohesive fracturing and stresses caused by hydration heat in massive concrete wall." *J. Eng. Mech.*, 129(1), 21–30.
- Bažant, Z. P., Kim, J.-K., and Panula, L. (1991). "Improved prediction model for time-dependent deformations of concrete: Part 1—Shrinkage." *Mater. Struct.*, 24(5), 327–345.
- Bažant, Z. P., Křístek, V., and Vitek, J. L. (1992). "Drying and cracking effects in box-girder bridge segment." *J. Struct. Eng.*, 118(1), 305–321.
- Bažant, Z. P., and Li, G.-H. (2008a). "Comprehensive database on concrete creep and shrinkage." *ACI Mater. J.*, 105(6), 635–639.

- Bažant, Z. P., and Li, G.-H. (2008b). "Unbiased statistical comparison of creep and shrinkage prediction models." *ACI Mater. J.*, 105(6), 610–621.
- Bažant, Z. P., Li, G.-H., and Yu, Q. (2009). "Prediction of creep and shrinkage and their effects in concrete structures: Critical appraisal." *Proc., 8th Int. Conf. on Creep, Shrinkage and Durability of Concrete and Concrete Structures*, Vol. 2, T. Tanabe, K. Sakata, H. Mihashi, R. Sato, K. Maekawa and H. Nakamura, eds., CRC, Boca Raton, FL, 1275–1289.
- Bažant, Z. P., Li, G.-H., Yu, Q., Klein, G., and Křístek, V. (2008). "Explanation of excessive long-time deflections of collapsed record-span box girder bridge in Palau." *Preliminary Structural Engineering Rep. 08-09/A222e*, Infrastructure Technology Institute, Northwestern Univ., Evanston, IL.
- Bažant, Z. P., and Liu, K.-L. (1985). "Random creep and shrinkage in structures: Sampling." *J. Struct. Eng.*, 111(5), 1113–1134.
- Bažant, Z. P., and Panula, L. (1978a). "Practical prediction of time-dependent deformations of concrete. Part I: Shrinkage." *Mater. Struct.*, 11(65), 307–316.
- Bažant, Z. P., and Panula, L. (1978b). "Practical prediction of time-dependent deformations of concrete. Part II: Basic creep." *Mater. Struct.*, 11(65), 317–328.
- Bažant, Z. P., and Panula, L. (1978c). "Practical prediction of time-dependent deformations of concrete. Part III: Drying creep." *Mater. Struct.*, 11(66), 415–424.
- Bažant, Z. P., and Panula, L. (1978d). "Practical prediction of time-dependent deformations of concrete. Part IV: Temperature effect on basic creep." *Mater. Struct.*, 11(66), 424–434.
- Bažant, Z. P., and Panula, L. (1979a). "Practical prediction of time-dependent deformations of concrete. Part V: Temperature effect on drying creep." *Mater. Struct.*, 12(69), 169–174.
- Bažant, Z. P., and Panula, L. (1979b). "Practical prediction of time-dependent deformations of concrete. Part VI: Cyclic creep, nonlinearity and statistical scatter." *Mater. Struct.*, 12(69), 175–183.
- Bažant, Z. P., Panula, L., Kim, J.-K., and Xi, Y. (1992). "Improved prediction model for time-dependent deformations of concrete: Part 6—Simplified code-type formulation." *Mater. Struct.*, 25(4), 219–223.
- Bažant, Z. P., and Prasannan, S. (1988). "Solidification theory for aging creep." *Cem. Concr. Res.*, 18(6), 923–932.
- Bažant, Z. P., and Prasannan, S. (1989a). "Solidification theory for concrete creep: I. Formulation." *J. Eng. Mech.*, 115(8), 1691–1703.
- Bažant, Z. P., and Prasannan, S. (1989b). "Solidification theory for concrete creep: II. Verification and application." *J. Eng. Mech.*, 115(8), 1704–1725.
- Bažant, Z. P., and Yu, Q. (2006). "Reliability, brittleness and fringe formulas in concrete design codes." *J. Struct. Eng.*, 132(1), 3–12.
- Bažant, Z. P., and Yu, Q. (2011). "Viscoplastic constitutive law for prestressing steel relaxation at varying strain." *Structural Engineering Rep. 11-03/ITIV*, Northwestern Univ., Evanston, IL.
- Bažant, Z. P., Yu, Q., and Li, G.-H. (2012). "Excessive long-time deflections of prestressed box girders. II: Numerical analysis and lessons learned." *J. Struct. Eng.*, 138(6), 687–696.
- Bažant, Z. P., Yu, Q., Li, G.-H., Klein, G., and Křístek, V. (2010). "Excessive deflections of record-span prestressed box girder: Lessons learned from the collapse of the Koror-Babeldaob Bridge in Palau." *Concr. Int.*, 32(6), 44–52.
- Berger/ABAM Engineers, Inc. (Berger/ABAM). (1995a). *Koror-Babeldaob Bridge modifications and repairs*.
- Berger/ABAM Engineers, Inc. (Berger/ABAM). (1995b). *Koror-Babeldaob Bridge Repaired Project Report on Evaluation of VECP, presented by Black Construction Corporation*.
- Brooks, J. J. (1984). "Accuracy of estimating long-term strains in concrete." *Mag. Concr. Res.*, 36(128), 131–145.
- Brooks, J. J. (2000). "Elasticity, creep, and shrinkage of concrete containing admixtures." *Proc., Adam Neville Symp. on Creep and Shrinkage—Structural Design Effects, ACI SP-194*, A. Al-Manaseer, ed., American Concrete Institute, Farmington Hills, MI, 283–360.
- Brooks, J. J. (2005). "30-year creep and shrinkage of concrete." *Mag. Concr. Res.*, 57(9), 545–556.
- Buckler, J. D., and Scribner, C. F. (1985). "Relaxation characteristics of prestressing strand." *Engineering Studies Rep. No. UILU-ENG-85-2011*, Univ. of Illinois, Urbana, IL.
- Burgoynne, C., and Scantlebury, R. (2006). "Why did Palau bridge collapse?" *Struct. Eng.*, 84, 30–37.
- Comité Euro-International du Béton (CEB). (1972). *Recommandations internationales pour le calcul et l'exécution des ouvrages en béton: Principes et recommandations*, CEB, Paris.
- Comité Euro-International du Béton—Fédération International de la Précontrainte (CEB-FIP). (1990). *CEB-FIP model code for concrete structures*, Thomas Telford, London.
- Cottrell, A. H. (1964). *The mechanical properties of matter*, Wiley, New York.
- DRC Consultants, Inc. (DRC). (1996). *Koror-Babelthup Bridge: Force distribution in bar tendons*.
- Fédération internationale de béton (fib). (1999). *Structural concrete: Textbook on behaviour, design and performance, updated knowledge of the of the CEB/FIP model code 1990*, Vol. 1, FIB, Lausanne, Switzerland, 35–52.
- Fédération internationale de béton (fib). (2010). *Draft of FIB model code*, FIB, Lausanne, Switzerland.
- Gardner, N. J. (2000). "Design provisions of shrinkage and creep of concrete." *Proc., Adam Neville Symp.: Creep and Shrinkage—Structural Design Effects, ACI SP-194*, A. Al-Manaseer, ed., American Concrete Institute, Farmington Hills, MI, 101–104.
- Gardner, N. J., and Lockman, M. J. (2001). "Design provisions for drying shrinkage and creep of normal strength concrete." *ACI Mater. J.*, 98(2), 159–167.
- Japan International Cooperation Agency (JICA). (1990). *Present condition survey of the Koror-Babelthup Bridge*, JICA, Tokyo.
- Japan Society of Civil Engineers (JSCE). (1991). *Standard specification for design and construction of concrete structure*, JSCE, Tokyo (in Japanese).
- Jirásek, M., and Bažant, Z. P. (2002). *Inelastic analysis of structures*, Wiley, New York.
- Křístek, V., and Bažant, Z. P. (1987). "Shear lag effect and uncertainty in concrete box girder creep." *J. Struct. Eng.*, 113(3), 557–574.
- Křístek, V., Bažant, Z. P., Zich, M., and Kohoutková, A. (2005). "Why is the initial trend of deflections of box girder bridges deceptive?" *Proc., 7th Int. Conf. on Creep, Shrinkage and Durability of Concrete and Concrete Structures (CONCREEP 7)*, Nantes, France, G. Pijaudier-Cabot, B. Gérard and P. Acker, eds., Hermes Science, London, 293–298.
- Křístek, V., Bažant, Z. P., Zich, M., and Kohoutková, A. (2006). "Box girder deflections: Why is the initial trend deceptive?" *ACI Concr. Int.*, 28(1), 55–63.
- Křístek, V., Vráblík, L., Bažant, Z. P., Li, G.-H., and Yu, Q. (2008). "Misprediction of long-time deflections of prestressed box girders: Causes, remedies and tendon lay-out effect." *Proc., 8th Int. Conf. Creep, Shrinkage and Durability Mechanics of Concrete and Concrete Structures (CONCREEP-8)*, Ise-Shima, Japan, R. Sato, K. Maekawa, T. Tanabe, K. Sakata, H. Nakamura and H. Mihashi, eds., Taylor & Francis, London, 1291–1295.
- Magura, D. D., Sozen, M. A., and Siess, C. P. (1964). "A study of stress relaxation in prestressing reinforcement." *PCI J.*, 9(2), 13–57.
- McDonald, B., Saraf, V., and Ross, B. (2003). "A spectacular collapse: The Koro-Babeldaob (Palau) balanced cantilever prestressed, post-tensioned bridge." *Indian Concr. J.*, 77(3), 955–962.
- Nawy, E. G. (2006). *Prestressed concrete: A fundamental approach*, 5th Ed., Section 3.3, Pearson Prentice Hall, Upper Saddle River, NJ.
- Nilson, A. H. (1987). *Design of prestressed concrete*, 2nd Ed., Wiley, New York.
- Parker, D. (1996). "Tropical overload." *New Civ. Eng.*, December, 18–21.
- Pilz, M. (1997). "The collapse of the KB bridge in 1996." Master's degree thesis, Imperial College, London.
- Pilz, M. (1999). "Untersuchungen zum einsturzter KB Brücke in Palau." *Beton- und Stahlbetonbau*, 94(5), 229–232.
- SSFEM Engineers, Inc. (SSFEM). (1996). "Preliminary assessment of Koror-Babeldaob Bridge failure." *Prepared for U.S. Army Corps of Engineers*, Washington, DC.
- T.Y. Lin International (TYLI). (1996). "Collapse of the Koror-Babelthup Bridge." *Rep.*, T.Y. Lin International, San Francisco.
- Yee, A. A. (1979). "Record span box girder bridge connects Pacific islands." *ACI Concr. Int.*, 1(6), 22–25.
- Yu, Q., Bažant, Z. P., and Wendner, R. (2012). "Improved algorithm for efficient and realistic creep analysis of large creep-sensitive concrete structures." *ACI Struct. J.*, in press.

Excessive Long-Time Deflections of Prestressed Box Girders. II: Numerical Analysis and Lessons Learned

Zdeněk P. Bažant¹; Qiang Yu²; and Guang-Hua Li³

Abstract: As a sequel to Part I, which clarified the causes of the unexpectedly large deflections of the Koror-Babeldaob Bridge in the Pacific island nation of Palau, Part II presents the numerical procedure and reviews the lessons learned. The box girder represents a thick shell that is discretized by eight-node, three-dimensional (3D) finite elements. Except for corrections due to cracking, concrete creep is assumed to follow aging linear viscoelasticity and is modeled by a rate-type law based on the Kelvin chain, the properties of which are adjusted for humidity conditions and temperature. In each time step and at each integration point, Widder's formula is used to convert the aging compliance function to a continuous retardation spectrum for the current age of concrete, and discretization of the spectrum yields the current elastic moduli of the Kelvin units. The shrinkage strains depend on the environmental humidity and the thickness of each plate in the cross section. The computations proceed according to Bažant's exponential algorithm, which is unconditionally stable and reduces the problem to a sequence of elasticity problems with an orthotropic effective stiffness of material and nonisotropic inelastic strains, different for each integration point in each time step. These problems are solved by commercial software ABAQUS. The segmental construction sequence is also modeled. The computer results reported in Part I explain the excessive deflections and compare the performance of various material models for creep and shrinkage. Part II formulates the lessons learned and makes recommendations for implementation. DOI: 10.1061/(ASCE)ST.1943-541X.0000375. © 2012 American Society of Civil Engineers.

CE Database subject headings: Creep; Shrinkage; Viscoelasticity; Deflection; Box girders; Numerical analysis; Prestressing.

Author keywords: Kelvin chain; Design standards; Segmental erection; Bridges; Shear lag; Prestressed concrete; Relaxation.

Introduction

The creep and shrinkage analysis of segmentally built prestressed concrete box girders is, in practice, often conducted in a rather simplified way. It usually relies on the material models recommended by the American Concrete Institute (ACI), Comité Euro-International du Béton/Fédération Internationale de Béton (CEB-FIP), and the Japan Society of Civil Engineers (JSCE), which grossly underestimate multidecade creep, give unrealistic shapes of creep and shrinkage curves and unrealistic effects of drying, and assume the creep to terminate at some fixed upper bound, for which no experimental support exists. In computer programs for long-time creep, the box girder is typically simplified as a beam with cross sections remaining plane, except that shear lag corrections for the effective width of top slab are usually made.

The previous analysis of the Koror-Babeldaob Bridge (hereafter, the KB Bridge) in Palau confirms that such simplifications are unrealistic. However, as demonstrated by the computer results in Part I, a significant improvement has been made possible by the advances

in material modeling of creep and shrinkage. The computational approach, which is usable for all box girder bridges, is presented here.

Creep Structural Analysis Utilizing ABAQUS

By step-by-step analysis, the structural creep problem gets reduced to a sequence of elastic finite-element analyses for an elastic stress-strain relation with inelastic strain, one analysis for each time step, which is an approach proposed in Bažant (1967). Because each such analysis can be carried out with a commercial finite-element program, one merely needs to find a suitable commercial finite-element program that has the requisite geometric and material modeling features. The software ABAQUS (Dassault Systèmes/SIMULIA; Providence, Rhode Island) has been chosen.

The plates (slabs and walls) of the box girder are subdivided into eight-node isoparametric finite elements (Fig. 1). Except in the top slab, the finite elements are chosen to extend through the whole thickness because the stresses caused by load do not vary significantly through the thickness and plate bending is not important. For drying creep and shrinkage, accurate modeling may generally require the wall thickness to be subdivided into at least six finite elements, but Model B3 makes it possible to avoid thickness subdivision because it is based on an analytical solution of drying according to the diffusion theory. This approach would not be accurate for cross sections subjected to flexure or highly eccentric compression, because the creep specimens in the underlying database are loaded centrally and are drying symmetrically. However, for the box girder, the accuracy is good because the resultant of normal stresses across the wall is everywhere nearly centric, the same as in standard creep tests.

In view of symmetry, only one-half of the bridge is analyzed. Together with the pier, it is subdivided into 5,036 hexahedral

¹McCormick Institute Professor and W. P. Murphy Professor of Civil Engineering and Materials Science, Northwestern Univ., 2145 Sheridan Road, CEE/A135, Evanston, IL 60208 (corresponding author). E-mail: z-bazant@northwestern.edu

²Assistant Professor, Dept. of Civil Engineering, Univ. of Pittsburgh, PA; formerly, Postdoctoral Research Associate, Northwestern Univ., Evanston, IL 60208.

³Graduate Research Assistant, Northwestern Univ., Evanston, IL 60208.

Note. This manuscript was submitted on February 1, 2010; approved on December 27, 2010; published online on May 15, 2012. Discussion period open until November 1, 2012; separate discussions must be submitted for individual papers. This paper is part of the *Journal of Structural Engineering*, Vol. 138, No. 6, June 1, 2012. ©ASCE, ISSN 0733-9445/2012/6-687-696/\$25.00.

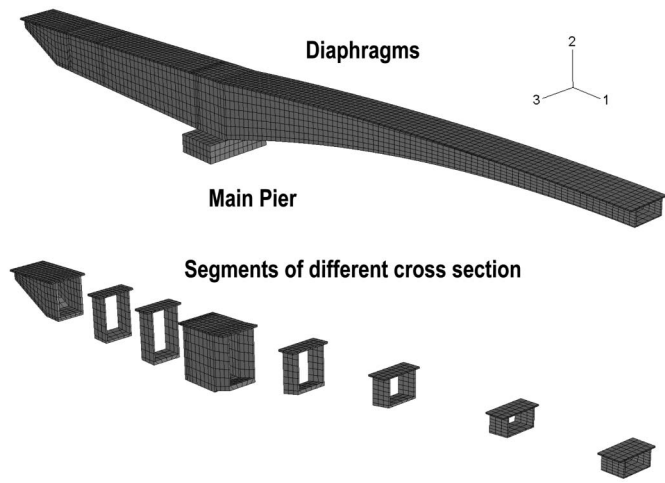


Fig. 1. Three-dimensionally meshed model of KB bridge and grouped segments

elements. The mesh, automatically generated by ABAQUS, is shown in Fig. 1. The prestressing tendons and the nonprestressed steel bars are further subdivided into 6,764 bar elements connected rigidly (with no slip) to the nodes of the three-dimensional (3D) mesh [the information on unprestressed steel is found in ABAM (1993)]. Sufficiency of mesh fineness has been validated by checking that a finer mesh with 20,144 hexahedral elements would yield only a negligible improvement of the computed elastic deflections.

The differences in the ages of various segments, the sequential prestressing at various times, and the stepwise load increase in the individual segments during construction (including the extra weight of 1,068 kN, or 240 kips, introduced during the construction by the formwork-carrying traveler) are taken into account according to the actual cantilever erection procedure. To simulate this segmental erection procedure, the elements are deactivated at first and then progressively reactivated according to the construction sequence (the ABAQUS keyword that enables this helpful feature is *Model change, Remove/Add*).

The individual prestressing bars, of which there are 316 above the main pier, were modeled as two-node line elements, attached to concrete at the nodes. The individual bars of unprestressed steel reinforcement were modeled similarly. The introduction of prestress was handled in ABAQUS automatically by the keyword *Initial conditions, type = stress, user* in the keyword editor. Thus, it sufficed to specify the prestress values of every tendon in the user subroutine *sigini* of ABAQUS. Although not all the tendons were prestressed fully at the same time (T. Y. Lin International 1996), each tendon was assumed to get fully prestressed 7 days after its anchoring segment had been cast. Capturing the time schedule accurately is important for the initial deflection history but not for multiyear deflections.

Because the tendons are straight, the curvature friction is nil and only the wobble friction was modeled. To do that, the initial prestress was diminished according to the length of each individual tendon using the wobble coefficient $\kappa = 0.0003/\text{ft}$ or $0.00098/\text{m}$ (e.g., Nilson 1987; DRC 1996).

The prestress losses caused by creep and shrinkage, by sequential prestressing of tendons, and by relaxation of steel stress, σ_s , are automatically reproduced by ABAQUS. For constant strain, ϵ , the relaxation is assumed to follow the CEB-FIB formula (CEB 1990) for prestress loss ratio: $\rho = (\sigma_0 - \sigma_s)/\sigma_0 = \rho_1(t/1,000 \text{ hours})^k$ where σ_0 = initial prestress, $k \approx 0.12$, and $\rho_1 \approx 6.5\%$ (value of ρ at 1,000 h). Because the strain in steel must be equal to the strain in adjacent concrete, which varies with

time t , this formula is generalized as (Bažant and Yu, “Viscoplastic constitutive law for prestressing steel relaxation at varying strain,” yet unpublished, 2012)

$$\dot{\epsilon} = \frac{\dot{\sigma}}{E_t} + \frac{k\rho_1^{1/k}A_T}{E_t\lambda_1} \frac{F(\epsilon)}{[1 - \sigma/F(\epsilon)]^{1/k-1}} = \frac{\dot{\sigma}}{E_t} + \frac{\sigma}{\eta} \quad (1)$$

$$\Delta\epsilon_v = \frac{\sigma}{\eta} \Delta t = \frac{k\rho_1^{1/k}A_T}{E_t\lambda_1} \frac{F(\epsilon)}{[1 - \sigma/F(\epsilon)]^{1/k-1}} \Delta t \quad (2)$$

where σ = current stress, $F(\epsilon)$ = stress at the short-time strain-stress curve for the initial prestressing, E_t = tangential modulus = $F'(\epsilon)$ (which is normally equal to E except for alloy bars with high prestress), and $A_T = \exp(Q/k_B T_0 - Q/k_B T)$ = Arrhenius temperature factor (Cottrell 1964), which equals 1 for room temperature $T_0 = 298\text{K}$, T = absolute temperature, Q = activation energy, k_B = Boltzmann constant, and $Q/k_B = 2,800\text{K}$ according to experimental data (fib 2010); for details, see Bažant and Yu (ibid.). For the KB Bridge, the tropical sunlight was considered to heat the pavement to about 55°C , and a simple calculation of heat conduction indicated that the top layer of tendons must have reached approximately 30°C within 2.5 h after pavement heating and for about 6 h daily. Based on the aforementioned value of Q/k_B , it was estimated that, as a time-averaged value, $A_T \approx 2$ for these tendons.

The foregoing stress-strain relation applies to tendon steel at any time step Δt . It is based on the Kelvin chain model for creep with stress-dependent viscosity and is implemented in the user subroutine *uexpan* of ABAQUS. For $\Delta\epsilon = 0$ or $\epsilon = \epsilon_0$, integration of Eq. (1) yields the CEB-FIB formula. Its validity is also verified by experiments (Magura et al. 1964; Buckler and Scribner 1985).

Effects of Slab Thickness, Temperature, and Cracking

Model B3 predicts separately the basic creep of the material (i.e., the part of creep unaffected by moisture content variation) and the additional effects of drying. These effects consist of the average shrinkage and average drying creep (or stress-induced shrinkage) in the cross section, and depend on the effective thickness, D , of the cross section.

The shrinkage is modeled by inelastic strain increments in the user subroutine *uexpan*. In each of the 25 segments of the central half-span, the plate thicknesses, D , and concrete ages are different, resulting in a different shrinkage function and a different compliance function for each plate of each segment.

Recent research (Křifstek et al. 2006) has revealed extreme sensitivity of box girder deflections to the differences in the rates of shrinkage and drying creep between the top and bottom slabs. Because Model B3 is physically based, the differences in its parameters between top and bottom can be assessed realistically, based on the known drying rates.

These rates are characterized by the shrinkage half-times, for which the diffusion theory gives the equation $\tau_{sh} = k_t(k_s D)^2$ [see Eq. (1.11) in Bažant and Baweja (2000)]; k_s = a shape parameter (= 1 for plates), and k_t = a permeability parameter for which a crude empirical estimate exists; $k_t = 0.03/C_1$ [see Eq. (28.12) in Jirásek and Bažant (2002)] where $C_1 = k_a P_1$ = diffusivity, $k_a \approx$ constant, and P_1 = permeability of concrete, which depends on temperature and the extent of cracking.

The mean temperature of the bottom slab and webs was probably 25°C (77°F), but during the day the top slab with the roadway layer—exposed on top to intense tropical sunlight—was probably

some 20°C (36°F) warmer. According to the curves for the temperature effect on permeability in Fig. 10.3(b, c) of Bažant and Kaplan (1996), this likely caused a tenfold decrease of τ_{sh} for the top slab. Furthermore, although no cracking could have occurred in the compressed bottom slab and webs, the top slab must have developed hairline cracks because it was under tension due to the excessive prestress loss. On the basis of the experiments reported (Bažant et al. 1987), cracks of 0.15-mm width will increase the drying rate by a factor of about 3. The same may be assumed for the top slab, and so, according to Eq. (1.20) of Bažant and Baweja (2000), the value of $k_t = 19.2$ is used for the bottom slab and the webs, and the value of $k_t = 19.2/30 = 0.64$ for the top slab. In calculations of deflections, the stiffness of the pavement layer is entirely neglected because it is unreinforced and in tension. However, because the pavement tends to decelerate the drying rate of the top slab, its effective thickness is taken into account in shrinkage modeling.

If V = volume and S = surface of a cross-section slice of the whole box, it used to be commonplace to consider one V/S value as a characteristic of the whole cross section, i.e., to take $D = 2V/S$. In that case, D was a property of the whole cross section, resulting in supposedly uniform shrinkage and supposedly uniform creep properties. However, Křístek et al. (2006) showed that, to avoid serious errors (which usually lead to overoptimistic interpretation of small, early deflections), differences in the drying rate attributable to different thicknesses D_i ($i = 1, 2, 3$) of the top slab, the bottom slab, and the webs must be taken into account.

A simple way to do that, demonstrated in Křístek et al. (2006), is to apply a model such as B3 separately to each plate of the cross section. Since the drying half-times are proportional to the square of slab thickness, the thickness differences then yield different shrinkage and different drying creep compliance in different plates.

According to models such as that of ACI, a thickness increase allegedly scales down the creep and shrinkage through a certain constant multiplicative factor, including the alleged final value for infinite time. However, in reality (except for a small multiplicative reduction due to a higher degree of hydration reached in thicker slabs), a thickness increase causes a delay, properly modeled as deceleration and characterized as an increase of the shrinkage half-time, which is proportional to the square of thickness (e.g., if the ultimate shrinkage for a slab 0.10 m or 4 in. thick is reached in 10 years, for a slab 1 m or 40 in. thick it is reached in 1,000 years, that is, virtually never).

Because of excessive prestress loss, the top slab is found to get into tension after the first year. Although no large tensile cracks were observed by JICA (1990), ABAM Engineers Inc. (1993) reported sparse fine cracks in the first six segments from the midspan. Calculations show that if the tensile strength limit, f'_t , is ignored, the tensile stresses in the top slab would in subsequent years reach the stress of about $2f'_t$, where f'_t = tensile strength, estimated as $6 \text{ psi} \sqrt{f'_c/\text{psi}} = 3.0 \text{ Mpa} = 433 \text{ psi}$. The most realistic model would be the cohesive crack model with rate-dependent softening, applied to growing parallel cracks of uniform spacing, with the material between the cracks considered as viscoelastic (Bažant and Li 1997). However, implementing this model with ABAQUS has been found to be virtually impossible.

After trying various simplifications with ABAQUS, the computations were eventually run under the simplifying assumption that the effective incremental modulus, E'' , for the current time step (which includes the effect of creep and is used in Steps 2 and 3 of the Appendix) gets reduced to $E''/4$ when the tensile stress exceeds $0.7 f'_t$ (Fig. 2). With this simplification, the maximum computed tensile stress in the top slab is about 3.0 MPa, and the corresponding strain is 1.83 times larger than the actual strain at peak tensile stress. With hardening due to positive $E''/4$

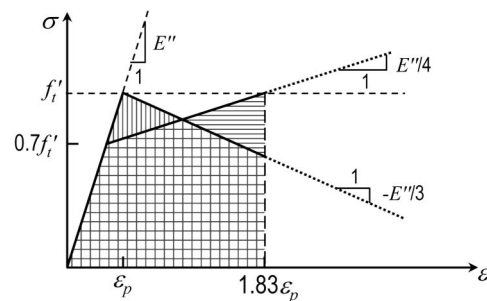


Fig. 2. Strain-stress relation if tensile strength is exceeded

compensated by the 70% strength reduction, the tensile stress resultant happens to be about the same as that obtained with a more realistic model consisting of a bilinear softening stress-strain relation with an unreduced tensile strength limit and the softening modulus of about $-E''/3$. The error compared with this more realistic model is estimated as $< 1\%$ of the deflection. In comparison, if unlimited tensile strength were assumed, the computed deflections would have been about 4% smaller.

Combined with the steel stiffness, the softening of concrete would have resulted in overall tension stiffening, which would have been easy to implement had all the computations been programmed. But in the algorithm with ABAQUS, the tensile softening turned out to be intractable because it would have interfered with the programming of the exponential algorithm for creep. This is why a positive modulus $E''/4$ had to be adopted.

Creep Analysis and Rate-Type Model Based on Kelvin Chain

The traditional characterization of concrete creep by the creep coefficient, giving the creep-to-elastic strain ratio, must be avoided (Bažant 1975, 1982; RILEM 1988; Bažant and Baweja 1995; Jirásek and Bažant 2002) because, due to pronounced short-time creep for durations > 0.0001 s, the definition of “elastic modulus” is ambiguous. Significant errors have often been caused by combining the creep coefficient with an incompatible value of the conventional elastic modulus. Thus, the analysis must properly be based on the compliance function $J(t, t')$, defined as the total strain ϵ_{xx} at age t caused by a sustained uniaxial stress $\sigma_{xx} = 1$ applied at age t' .

An individual material constitutive law corresponding to every different creep and shrinkage prediction model has been developed for the user subroutine *umat* of ABAQUS. The three-dimensional generalization is obtained under the assumption of material isotropy; and a time-independent Poisson ratio, ν (Bažant 1975, 1982; RILEM 1988); $\nu = 0.21$ is used here, based on core sample tests (Berger/ABAM 1995). Linear viscoelasticity implies the principle of superposition in time, the direct application of which gives the stress-strain relation in the form of a history integral. However, major deviations from the principle of superposition are caused by tensile cracking and by time variations of humidity and temperature (and also by triaxial damage in compression, which, however, can be ignored for service states). Therefore, the history integrals are inapplicable and the corrections for cracking, for example, must be introduced after converting the compliance function to an equivalent rate-type creep law, which is here based on the Kelvin chain model. This conversion also greatly improves computational efficiency.

In the case of Model B3, conversion of the compliance function of basic creep to a rate-type creep law is particularly easy. It can be done according to the solidification theory (Bažant and Prasanna 1988, 1989a, b; Jirásek and Bažant 2002), in which the aging is

taken into account by means of volume growth of the solidifying component and by a gradual increase with age of the flow term viscosity. Thus, it is possible to use a nonaging compliance function for the solidifying component, for which one can uniquely determine a continuous retardation spectrum. This spectrum can be readily obtained from Widder's formula (Tschoegl 1989), a simple, explicit formula that is based on the inversion of the Laplace transform (Bažant and Xi 1995). The parameters of the Kelvin chain model are in this case constant (i.e., nonaging) and are simply obtained as a discrete representation of the continuous spectrum.

For empirical models, such as those of ACI, CEB, JSCE, and Gardner-Lockman (GL) (ACI 2008), such an approach is impossible because a nonaging constituent in the sense of the solidification theory cannot be identified for these models. Therefore, compliance curves that change with the age at loading must be used, as defined by $J(t, t')$. This problem was handled in the 1970s by considering the retardation (or relaxation) spectrum to be age-dependent, which meant that the spectrum of elastic moduli $E_\mu(t)$ ($\mu = 1, 2, 3, \dots$) of the Kelvin (or Maxwell) chain model had to be considered as age-dependent, too (Bažant 1975, 1982; RILEM 1988). Unfortunately, the least-squares identification of these moduli as functions of age appeared to be an ill-conditioned problem because different functions $E_\mu(t)$ provided almost equally good fits of $J(t, t')$, even if they were not increasing monotonically as required by aging.

An age-independent spectrum can nevertheless be used within each sufficiently short time step, such that the creep properties, including the moduli and viscosities of the Kelvin chain model, could be considered to be approximately age-independent, corresponding to concrete age $t_{n-1/2}$ in the middle of the time step. Indeed, for the stress changes within a short enough time step, the concrete may be considered to behave as a nonaging, linearly viscoelastic material characterized by the Kelvin chain moduli and viscosities corresponding to age $t_{n-1/2}$, which depend only on the compliance curve $J_{n-1/2}(t) = J(t, t_{n-1/2})$. This curve corresponds to one retardation spectrum and is approximated by one Kelvin chain, having constant moduli $E_\mu(t_{n-1/2})$ ($\mu = 1, 2, 3, \dots$), applicable to the current time step only.

For the average age $t_{n-1/2}$ corresponding to every time step, the compliance curve $J_{n-1/2}(t)$ corresponding to, for example, the ACI, CEB, or GL model, one must identify the corresponding retardation spectrum corresponding to age $t_{n-1/2}$. This can be done according to Widder's explicit formula (Bažant and Xi 1995), before starting the step-by-step finite-element analysis of the structure. This continuous retardation spectrum is approximated by a set of discrete spectral values, E_μ , a different set for each time step. These spectral values are then used in the individual time steps of Bažant's exponential algorithm based on the Kelvin chain (as described in Bažant 1971, 1975, 1982; RILEM 1988; Jirásek and Bažant 2002).

For example, the ACI compliance function (ACI 1971), which reads $J(t, t') = \psi(t')f(\xi)$, where $\xi = t - t'$ and $f(\xi) = \xi^{0.6} / (10 + \xi^{0.6})$, can be approximated by a continuous retardation spectrum (Bažant and Xi 1995) for a fixed value of the given aging function, $\psi(t')$:

$$\begin{aligned}
 A_\mu &= \psi(t')L(\tau_\mu)\Delta(\log \tau_\mu) \ln 10, \\
 L(\tau_\mu) &= -\lim_{k \rightarrow \infty} \frac{(-k\tau_\mu)^k}{(k-1)!} f^{(k)}(k\tau_\mu)
 \end{aligned} \tag{3}$$

where k is a positive integer, and $f^{(k)}$ is a k th-order derivative of function $f(\xi)$ ($k = 3$ usually suffices for good accuracy).

In Fig. 3 (top), two sets of constant moduli of the Kelvin chain obtained by approximating the continuous spectrum are used to

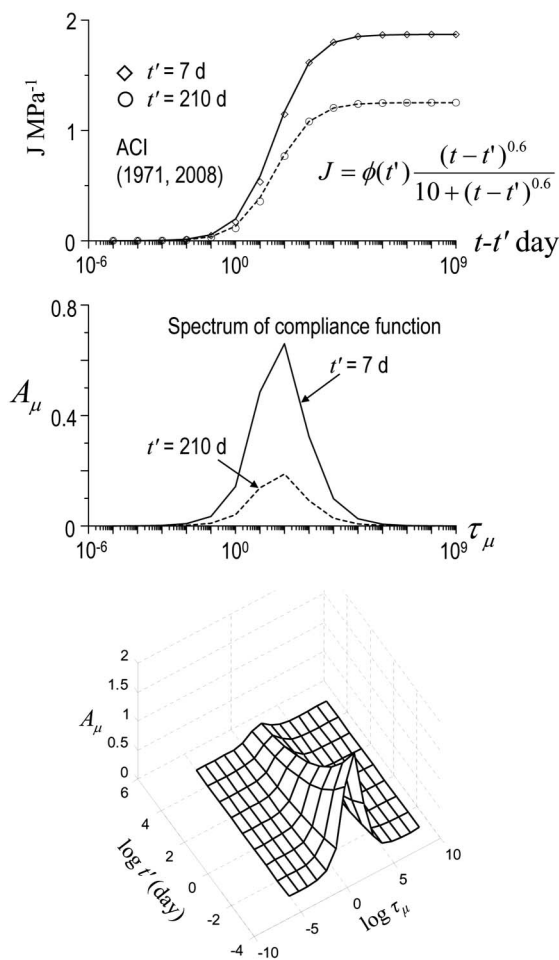


Fig. 3. Retardation spectra of ACI model

approximate the compliance function, $J(t, t')$, corresponding to sustained stress applied at age $t' = 7$ days (diamond points) or 210 days (circle points). The difference from the $J(t, t')$ curves is negligible compared with the ACI model. In advance of the step-by-step finite-element analysis, the spectrum and the corresponding set of Kelvin chain moduli, E_μ , are identified from the given compliance function for the center of each time step.

The corresponding spectra A_μ ($\mu = 1, 2, 3, \dots$) are also plotted in Fig. 3 (middle). Note that in each case the spectrum, A_μ , approaches 0 as the retardation time, τ_μ , increases. The reason is that the creep strain expressed by the ACI model is bounded, with the creep rate essentially vanishing after 10 years [this is, of course, contradicted by long-term creep test results, as reported by, Brooks (1984, 2005), for example]. The surface of the continuous spectra, $A_\mu = 1/E_\mu$, that closely approximates the ACI compliance function for different ages at loading is exemplified in Fig. 3 (bottom), where the coordinates are the retardation times, τ_μ , and the ages t' . For the CEB, JSCE, and GL models, the procedure is similar.

For Model B3, which is based on solidification theory, the moduli of the Kelvin chain are constant but only for basic creep. As demonstrated in Fig. 4 (top), the creep compliances for ages, $t' = 7$ days (diamonds) and 210 days (circles), can be closely approximated by the same nonaging spectrum, which is plotted in the middle of Fig. 4. In addition to the basic creep, there is in Model B3 a separate drying creep term, which captures the Pickett effect. This term applies only to the in-plane directions, so different compliance functions had to be obtained for the in-plane and transverse directions of the plates. The drying creep term of Model B3 applies only

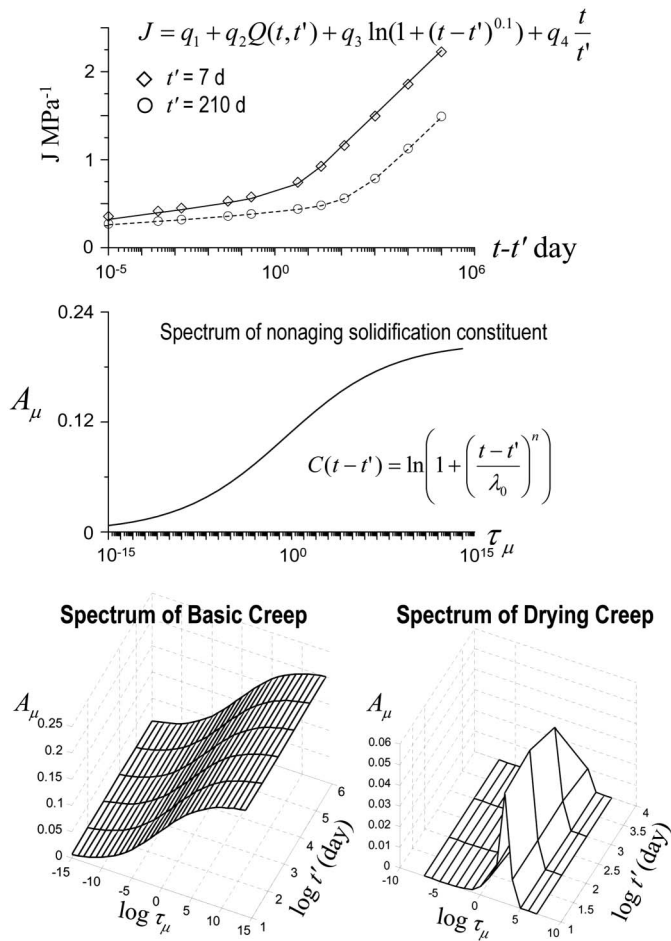


Fig. 4. Retardation spectrum of Model B3

to the normal strains and causes no Poisson effect. These distinctions cannot be made for the other models. Unlike the basic creep, which is unbounded, the drying creep is bounded. Like the shrinkage, it depends on humidity and cross-section thickness.

The microprestress-solidification theory (Bažant et al. 1997) would have been more realistic for representing both the drying creep and aging. However, it would have required calculating the distributions of pore relative humidity across the thickness of each slab, which would have necessitated not one but at least six finite elements over the slab thickness.

In Model B3, the drying creep is approximated by the compliance function

$$C_d(t, t', t_c) = q_5 \sqrt{e^{-8H(t)} - e^{-8H(t')}} \quad (4)$$

$$H(x) = 1 - (1 - h) \tanh \sqrt{\frac{x - t_c}{\tau_{sh}}}$$

where t = current age of concrete, t' = age at loading, t_c = curing time, h = relative humidity, and τ_{sh} = shrinkage halftime. As shown in Eq. (4), a nonaging spectrum cannot be identified to approximate the drying creep. Therefore, an age-dependent spectrum similar to Eq. (3) is calculated. The spectrum A_μ , describing the drying creep, is plotted in Fig. 4 (bottom). This age-dependent spectrum approaches zero as the retardation time, τ_μ , increases because the drying creep is bounded. Contrary to the nonaging spectrum for basic creep, it reaches a finite value as τ_μ increases. Therefore, the overall asymptotic long-time creep predicted by Model B3 will follow a constant slope when plotted in the logarithmic scale.

In previous research (Bažant 2000) and the current study, the models other than B3 exhibit some serious deficiencies, theoretical as well as practical. One deficiency, especially for the ACI and CEB models, is that the long-time creep is strongly underestimated. Other deficiencies of the ACI model and, to a lesser extent, the CEB model, are that the drying creep, which is very sensitive to the cross-section thickness, is not separated from the basic creep and that the effects of thickness on shrinkage and on drying creep are described by a scaling factor rather than by a time delay (Bažant 2000).

After the Kelvin chain moduli for the current time step, Δt , and the current integration point are obtained, the exponential algorithm (Bažant 1975, 1982; RILEM 1988; Jirásek and Bažant 2002) is implemented. It was derived as the exact solution for stress varying linearly within Δt (Bažant 1971). Although the standard central or backward difference algorithm becomes numerically unstable for Δt exceeding the shortest τ_μ , this algorithm is unconditionally stable. The initial time steps, Δt , after the hinge installation at mid-span were 0.1, 1, 10, and 100 days. After that, Δt was kept constant at 100 days up to 19 years. For the deflection prediction up to 150 years, all the subsequent time steps (Δt) were 1,000 days. Although time steps increasing in geometric progression would have been computationally more efficient, they would not have matched the times of deflection measurements.

Comparison to Bending Theory with Plane Cross Sections

The existing computer programs for creep effects assume that the prestressed concrete box girders follow the engineering theory of bending, which presumes the cross sections of the box to remain planar and normal to the deflection curve. However, this theory is too simplified to capture the 3D deformation of box girders. The main deficiency is that it misses significant shear lag effect in the top slab, in the webs, and in the bottom plate, each of which is different for the self-weight and for the prestress loads from tendon anchors. Fig. 5 shows the distribution of normal and shear stress in the cross section located at 14.63 m (48 ft) from the main pier under self-weight and in the cross section at 60.35 m (198 ft) from the main pier under prestress.

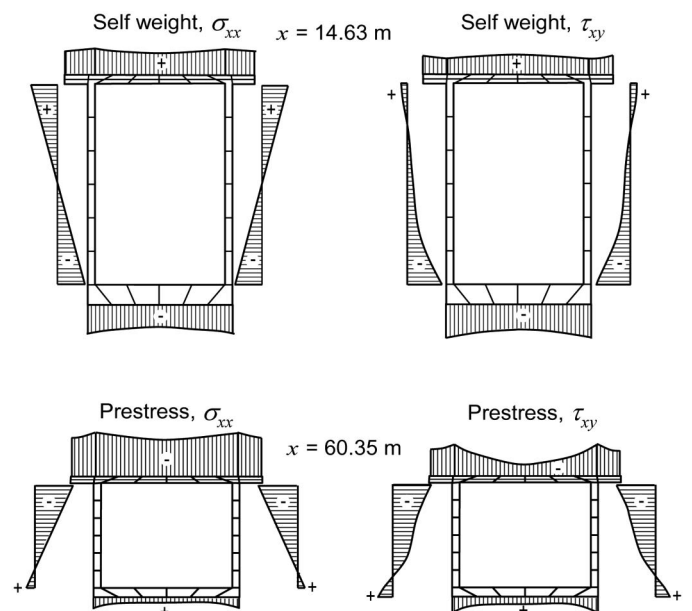


Fig. 5. Stress distribution in the cross section at different locations

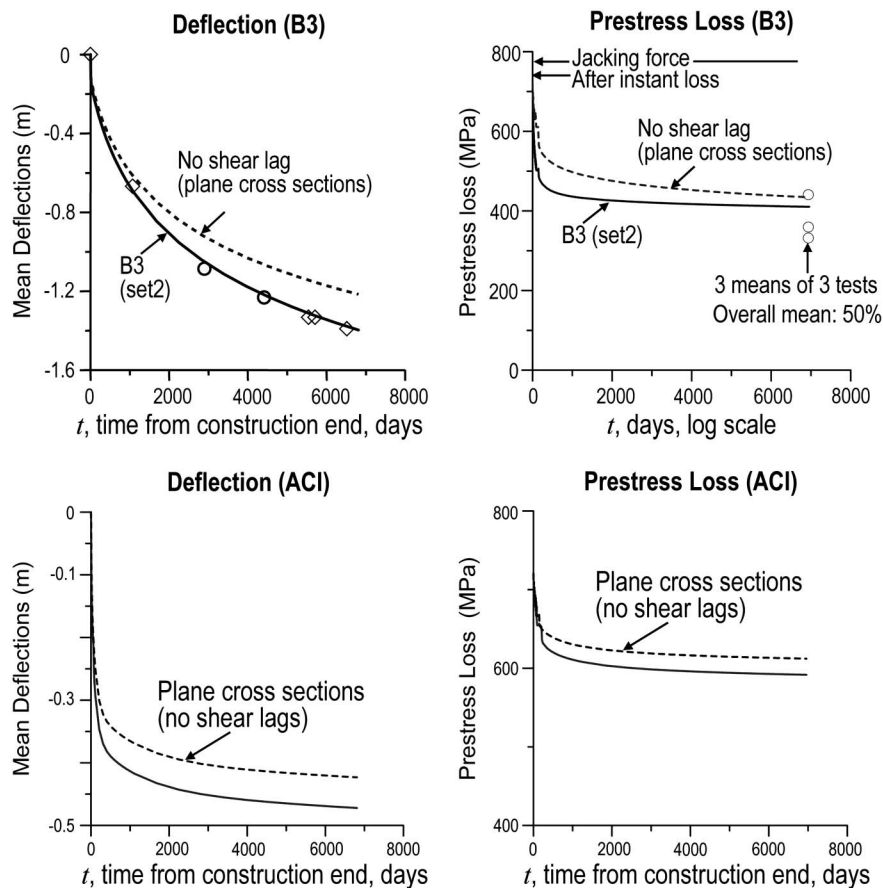


Fig. 6. Comparison of deflections obtained by full 3D analysis with deflections obtained according to the bending theory with cross sections remaining plane

A strong sensitivity to errors occurs because the bridge deflection represents a small difference between two large, statistically uncertain, numbers—the downward deflection caused by the self-weight and the upward deflection attributable to the prestress. The shear lag plays a relatively more important role in the former. The error caused by neglecting the shear lags is thus magnified.

Fig. 6 shows that the discrepancy between the full 3D analysis and the analysis based on the engineering theory of bending is significant. The deflections and prestress losses for both cases are compared using the B3 and ACI models. Compared with the 3D analysis, the analysis using the classical bending theory is found to underpredict the deflection by about 20%.

In the KB Bridge design, an approximate correction for the shear lag in the top slab attributable to self-weight was introduced (Khaled Shawwaf, former structural analyst on KB Bridge design team and currently a director at Dywidag Systems International USA, Bolingbrook, Illinois; personal communication, September 18, 2008) through the classical effective width concept (Reissner 1946; Benscoter 1954; Abdel-Samad et al. 1968; Malcolm and Redwood 1970; Richtlinien 1973). However, these classical formulas are not very accurate and still miss the shear lags in the webs and bottom slabs and those due to prestress forces. This causes a significant error.

Cyclic Creep and Its Structural Effect

In discussions at various conferences it has often been claimed that the cyclic creep caused by repeated traffic loads may explain the excessive long-time deflection. Let us examine this claim.

As argued in Bažant and Kim (1992), the cyclic creep caused by repeated traffic loads may best be represented as an acceleration of the basic creep attributable to the sustained load. The acceleration of creep by a compressive stress cycled between limits σ_{\min} and σ_{\max} may be represented as a forward shift, Δt_N , of the time for which the deformations are evaluated. A recent investigation (not yet published) found that the empirical formula proposed in Bažant and Kim (1992) was contaminated by lack of separation of fatigue data for high stress levels. The corrected empirical formula for the time shift can be expressed as

$$\Delta t_N = k_c N \Delta^q \sigma_{\max}^p f_0^{l-q-p} \quad (5)$$

where f_0' = compressive strength at the time of loading (estimated as 25.2 MPa, or 3,658 psi for the KB Bridge); $\Delta = \sigma_{\max} - \sigma_{\min}$; N = total number of cycles during $t - t'$; q and p = dimensionless constants; k_c = constant of the inverse unit of supplied frequency, e.g., day. When $k_c = 0.0038$ day, $p = 0$, and $q = 3.54$, Eq. (5) gives the best fitting of test data for sealed specimens.

At the centroid of the bottom slab at the face of the pier, $\sigma_{\min} = 7.50$ MPa (1,088 psi). The most important traffic loads are heavy trucks, considered to weigh about 20 tons (44,092 lb). The stress caused by each of them is calculated to be about 0.21 MPa (30.5 psi), so $\sigma_{\max} = 7.71$ MPa (1,118.5 psi). It is estimated that only about 1 million such trucks passed over the KB Bridge within 18 years (i.e., $N = 10^6$). For the KB Bridge, the intervals between such heavy trucks were so long that the time average of the cyclic stress component was negligible and $\bar{\sigma} \approx \sigma_{\min}$ = stress caused by

all permanent loads (self-weight, prestress, and additional dead load). Substitution of these numbers into Eq. (5) yields

$$\Delta t_N = 10^6 \times 0.0038 \text{ days} \times (0.21/25.2)^{3.54} = 0.00017(\text{days}) \quad (6)$$

Thus, the effect of cyclic creep attributable to the heavy trucks is equivalent to extending the duration of static creep by about 14 s. In this calculation, it was assumed that only one 20-ton truck would appear at the midspan at a given time. The number of simultaneous occurrences of two or three such trucks at the midspan is estimated to be $N = 10,000$ or $1,000$, respectively (during 18 years), and similar calculations then show that the cyclic creep produced is equivalent to extending the static creep duration by 1.67 s or 0.7 s, respectively.

Traffic observations further showed that about 200 regular cars, of about 3 tons each, passed over the bridge per hour during daytime. This gives $N = 16$ million car passages in 18 years. Similar calculations give the extension of 0.3 s.

All these extensions together amount to about 17 s of static creep for the cross section at the face of the pier. From this, one can determine the additional cyclic creep strain in the bottom plate.

Similar calculations can be repeated for the forward time shifts of cyclic creep strain history at various points of the web and top plate of the cross section at the face of the pier. Because both σ_{\max} and Δ are smaller, the forward shift of the creep history at these points will be less than 17 s. Hence, 17 s is the upper bound for the forward shift of the curvature history of the girder at this cross section. Calculations for the quarter-span cross section give a slightly longer time shift, but the effect of curvature increase on the midspan deflection is, for the quarter-span cross section, much smaller than it is for the cross section at the pier face. Consequently, the upper bound on the forward time shift of the midspan deflection history should be roughly the same as the upper bound on the shift of the curvature history in the cross section at the pier face. Looking at the terminal slope of the deflection curve of the bridge in Fig. 4 of Part I, which is about 1 m per 15,000 days, one concludes that the cyclic creep increased the midspan deflection by not more than $1 \text{ m} \times 0.0002/15,000 \approx 0 \text{ m}$.

For bridges of shorter spans, in which the self-weight represents a smaller portion of the load, the stress cycles span over a greater portion of stress range and their effect is magnified by high exponent q in Eq. (5). Then the cyclic creep effect can be more important, although hardly major. For example, the Nusle Valley Bridge in Prague (Bažant 1968a, b), which has spans of 102 m and carries a much heavier traffic load (subway trains inside the box in addition to cars on top) was analyzed (by a different method) in 1966. It was concluded that the cyclic creep would increase the deflection of that bridge by only 4 cm (Bažant 1968b).

The present model of cyclic creep analysis was formulated in Bažant and Panula (1979), refined in Bažant and Kim (1992), and improved recently. Eq. (5) was also validated by comparisons with the main existing data (Gaede 1962; Kern and Mehmel 1962; Whaley and Neville 1973; Suter and Mickleborough 1975; Hirst and Neville 1977). Note that the present cyclic creep correction cannot be applied to the ACI, CEB, and JSCE models. They would give a zero effect of cyclic creep because the creep load-deflection curve terminates with a horizontal asymptote.

This analysis also brings about another interesting point. Because (aside from the nonlinear corrections for drying and cracking) the principle of superposition is the basis of creep analysis, the time average of traffic loads should be included in the permanent loads. So, the effect of cyclic creep, which can be neglected for traffic loads of low frequency and small amplitude, might be non-negligible for bridges with many lanes, with both a highway and a railroad, or with a dense traffic of heavy trucks.

Lessons Learned and Recommendations

1. As a purely predictive tool, none of the available material models for predicting creep and shrinkage is satisfactory.
2. The 1971 ACI model (reapproved in 2008) (ACI 2008) and, to a somewhat lesser extent, the CEB and JSCE models, severely underestimate multidecade deflections as well as the prestress losses and give an unrealistic shape of deflection histories. The recent GL model (ACI 2008) gives better predictions but not sufficiently better. None of these models has free intrinsic input parameters to be updated from experiments or to explore the range of possible responses, and none can take temperature into account.
3. Model B3, which is, to a large extent, theoretically based and has been calibrated by filtering out the database bias for short durations and ages, gives significantly better multidecade predictions of the deflection history and its shape, and of the deflection growth rate.
4. Even Model B3 is unsatisfactory when its input parameters are estimated from the composition of concrete or taken at their default values. However, because of its free parameters, Model B3 can be made to fit the measurements perfectly with input parameters that are within their realistic ranges, agreeing with the long-term test data that exist. Thus, the form of Model B3 appears to be correct, and the problem is with the empirical formulas predicting the input parameters from the composition of concrete. Obviously, these formulas should be improved.
5. The box girders are thick-walled shells for which the beam-type analysis is inadequate. Three-dimensional analysis must be used. Its main purpose is to capture the shear lag effects, which are different for self-weight and for the loads from prestressing tendons, and occur not only in the top slab but also in the webs and the bottom slab. At the piers, the self-weight produces large vertical shear forces in the web, while the prestress does not; the loads from tendon anchors produce shear lags mainly in the top slab. The shear lag for the self-weight is stronger than it is for the prestress. Because the total deflection is a small difference of two large statistically uncertain numbers—one for the downward deflection caused by self-weight and the other for the upward deflection caused by prestress—small percentage errors in each (typically ± 10 – 15%) will result in a far larger percentage error in the total deflection.
6. For box girders wider than the KB Bridge (which had only two lanes), the difference between the beam-type analysis of creep and shrinkage and the 3D analysis, which captures the shear lag effects, must be expected to be larger.
7. The effect of thickness differences among the webs and the top and bottom slabs on the drying shrinkage and drying creep must be taken into account. This leads to nonuniform creep and shrinkage properties throughout the cross section, manifested as differential drying creep compliances and differential shrinkage.
8. For the tendons embedded in the top slab, the periodic heating by sunlight may significantly intensify the steel stress relaxation, which in turn may appreciably increase the deflections.
9. In the creep and shrinkage prediction model, the drying creep should be separated from the basic creep, because the former is thickness-dependent and approaches a finite terminal value, whereas the latter is thickness-independent and unbounded. Only Model B3 has this feature. As evidenced by the KB Bridge, the thickness-induced differences in the compliance functions for drying creep can be more important than those in shrinkage.
10. The prestress loss in box girders can be two to three times higher than predicted by simple textbook formulas or lump estimates. It can also be much higher than that calculated by

the theory of beam bending, in which the cross sections are assumed to remain plane. It should be calculated as part of the 3D finite-element analysis of stresses and deflections.

11. When dealing with large, creep-sensitive structures, the creep and shrinkage prediction model must be updated by means of short-time tests of the creep and shrinkage of the given concrete. The updating is effective only if the curves of creep and shrinkage growth have correct shapes for short times, which is the case only for Model B3.
12. The shrinkage tests must be accompanied by simultaneous measurements of water loss caused by drying (Bažant and Baweja 1995, 2000); otherwise, the extrapolations can have errors of the order of 100% [the value of such tests has been demonstrated for some recent large bridges; Navrátil (1998)]. B3 is a model that has been specifically formulated to allow easy updating by linear regression, whereas the updating problem is nonlinear for other models.
13. Large bridges should be designed not for the mean but for the 95% confidence limit on the predicted deflection (in other words, having to repair or close only 1 among 20 similar bridges is acceptable, but 10 is not). The necessary statistical analysis is easy. It suffices to repeat a deterministic computer run of structural response about 10 times, using random samples of the input parameters. Since the distribution of structural response can be assumed to be normal, it suffices to obtain from the structural responses only the mean and the coefficient of variation.
14. As observed in a previous study (Křístek et al. 2006), the deflection evolution of large box girders is usually counterintuitive. The deflections at first grow slowly or are even negative, which may lead to unwarranted optimism, but after a few years a rapid and excessive deflection growth sets in. The early deflections of the KB Bridge were not measured, but according to the present computer simulations with nonsymmetric drying, the deflection growth of this bridge must have been very slow during the first year (Fig. 3 in Part I).
15. In design, it is prudent to minimize deflections and prestress losses by the following measures, most of which are well known though often not followed: (1) avoid midspan hinge; (2) choose a concrete with a low long-time creep; (3) use a tendon layout that minimizes deflections (Křístek et al. 2008); (4) give concrete more time to gain strength before prestressing; (5) increase the level of prestress, preferably so high that an upward deflection be predicted; (6) use stiffer (deeper) girders; and (7) install empty ducts for possible later installation of additional tendons.

Appendix. Algorithm and Numerical Implementation

Algorithm Utilizing ABAQUS (Applicable to All Creep Models)

1. For each integration point of each finite element, specify effective slab thickness, t_b , relative humidity, h , and temperature, T (but, if h and T vary, they must be updated at the start of each time step). For curing time $t = t_c$, initialize the 6×1 vector (column matrix) of shrinkage strains ϵ_s^0 . For $t = t_0$, initialize the internal variables $\gamma_\mu^{(0)} = 0$ ($\mu = 1, \dots, N$) and $J(t_0, t_0) = 1/E_0$ ($E_0 =$ conventional short-time elastic modulus, except that for the B3 model $E_0 = 1/q_1 =$ asymptotic modulus). Select the discrete retardation times $\tau_\mu = 10^{\mu-7}$, $\mu = 1, 2, \dots, N$, where, for lifespan < 250 years, $N = 13$ satisfies the condition that $10^{N-7} \approx 10 \times$ lifespan (see Note I).

2. Loop over time steps (separated by discrete times $t_n, n = 1, 2, \dots$). Set $\Delta t = t_n - t_{n-1}$, and $t_{n-1/2} = t_0 + [(t_n - t_0)(t_{n-1} - t_0)]^{1/2}$ for $n > 1$. For $n = 1$, $t_{1/2} = (t_0 + t_1)/2$.
3. Loop over finite elements and their integration points.
4. Calculate the increment of 6×1 shrinkage strain vector $\Delta \epsilon_s = \epsilon_s(t_n) - \epsilon_s(t_{n-1})$ from t_b, h , and T in user subroutine *uexpn*.
5. Supply current stress $\sigma^{(n-1)}$ and strain increment $\Delta \epsilon = \Delta \epsilon^{total} - \Delta \epsilon_s$ calculated by ABAQUS to the user material subroutine in *umat*, in which Bažant's exponential algorithm is implemented.
6. Use Widder's formula $L(\tau_\mu) = -\lim_{k \rightarrow \infty} (-k\tau_\mu)^k C^{(k)}(k\tau_\mu) / [(k-1)!]^{-1}$ to calculate the continuous retardation spectrum; here $C^{(k)}$ = k th derivative on t of the creep part $C(t, t_{n-1/2})$ of compliance function, $C = J - 1/E_0$ (usually $k = 3$ suffices for good approximation). Determine the discretized spectrum $A(\tau_\mu) = L(\tau_\mu) \ln 10 \Delta(\log \tau_\mu) = L(\tau_\mu) \ln 10$. Calculate $\beta_\mu = e^{-\Delta t / \tau_\mu}$, $\lambda_\mu = \tau_\mu(1 - \beta_\mu) / \Delta t$, $D_\mu = [A(\tau_\mu)(1 - \lambda_\mu)]^{-1}$; incremental modulus $E''(t_{n-1/2}) = [E_0^{-1} + \sum_{\mu=1}^N D_\mu^{-1}]^{-1}$.
7. Compute the inelastic (creep) strain increment vector $\Delta \epsilon'' = \sum_{\mu=1}^N (1 - \beta_\mu) \gamma_\mu^{(n-1)}$.
8. Supply to ABAQUS for this integration point the 6×6 incremental quasielastic matrix stress-strain relation $\Delta \sigma = E'' \mathbf{D}(\Delta \epsilon - \Delta \epsilon'')$ where \mathbf{D} is a constant 6×6 matrix for isotropic material with given Poisson ratio ν .
9. Check the tensile strength limit $\sigma_i \leq f'_t$ ($\sigma_i =$ principal stresses, $i = 1, 2, 3$). If exceeded, reduce the stress according to the specified postpeak behavior (although usually unnecessary, the compressive damage could also be included here).
10. End of loops over finite elements and over their integration points.
11. Run with ABAQUS the elastic finite-element analysis, in which each integration point has generally a different elastic moduli matrix and different inelastic strains.
12. Update the internal variable vectors $\gamma_\mu^{(n)} = \lambda_\mu \Delta \sigma D_\mu^{-1} + \beta_\mu \gamma_\mu^{(n-1)}$.
13. End of loops over finite elements and their integration points, and go to Step 2 and begin the next time step.
14. End of loop over time steps.

Note I: The number N of internal variables could actually be reduced to about five to seven, but then the first $L(\tau_\mu)$ would have to be computed as the integrated area under the spectrum up to $-\infty$ in the log-time scale (the reason is that Kelvin units with $\tau_\mu \ll \Delta t$ behave as springs, the compliances of which can thus be combined into one compliance). Using $N = 22$ for Model B3 and $N = 13$ for other models increases the demand on computer time and storage but is simpler to program. The spectral values $L(\tau_\mu)$ for $\tau_\mu \gg t$ can be ignored because the corresponding Kelvin units behave as perfectly rigid.

Exponential Algorithm Simplifications for Model B3

The foregoing algorithm can be used for Model B3 if $j(t, t')$ is computed for each integration point. However, for basic creep, there exists a simpler exponential algorithm (Bažant and Prasanna 1989a, b), which needs only the compliance rate $\dot{J}(t, t')$ and is applied only to the nonaging viscoelasticity of the nonaging constituent of growing volume. The following steps are then modified:

In Step 1, $\mu^b = 1, 2, \dots, N^b$, $\tau_\mu^b = 10^{-15+\mu^b}$, and $\mu^d = 1, 2, \dots, N^d$, $\tau_\mu^d = 10^{-7+\mu^d}$. Here $N^b = 22$ and $N^d = 15$ ($\tau^b, \tau^d =$ retardation times for basic creep and drying creep).

In Step 6, for basic creep, replace $A(\tau_\mu)$ with $A^b(\tau_\mu^b) = (\sqrt{1/t_{n-1/2}} + q_3/q_2) \times A(\tau_\mu^b)$, where $A^b(\tau_\mu^b)$ is the discretized spectrum for basic creep.

In Step 7, $\Delta\epsilon'' = \sum_{\mu=1}^{N_b} \left(\sqrt{1/t_{n-1/2}} + q_3/q_2 \right) \times (1 - \beta_{\mu})\gamma_{\mu}^{(n-1)} + \sum_{\mu=1}^{N_d} (1 - \beta_{\mu})\gamma_{\mu}^{(n-1)}$.

After Step 7, add the strain increment due to the viscous flow: $\Delta\epsilon'' = \Delta\epsilon'' + q_4\sigma^{(n-1)}\Delta t/t_{n-1/2}$.

Implementation Example Using ACI-209 Model

For the ACI model, $J(t, t') = (1 + \varphi(t, t'))/E(t')$, $\varphi(t, t') = 2.35\gamma_c(t - t')^{0.6}/[10 + (t - t')^{0.6}]$, where γ_c = empirical factor accounting for age t' at loading, humidity, slab thickness, slump of fresh concrete, and contents of fine aggregates and of air. In ABAQUS, the exponential algorithm is used in the user material subroutine:

1. At $t = t_0$, initialize the internal variables: $\gamma_{\mu}^{(0)} = 0$, $J(t_0, t_0) = 1/E(t_0)$ where t_0 = time when the first load is applied. Select $\tau_{\mu} = 10^{-7+\mu}$ ($\mu = 1, 2, \dots, 13$). Use Widder's formula to calculate the continuous spectrum: $d^3\varphi/d\xi^3 = \psi(\xi) = 2.35\gamma_c[0.336\xi^{-2.4}(10 + \xi^{0.6})^{-1} + 0.528\xi^{-1.8}(10 + \xi^{0.6})^{-2} + 0.432\xi^{-1.2}(10 + \xi^{0.6})^{-3} - 1.296\xi^{-0.6}(10 + \xi^{0.6})^{-4}]$, where $\xi = t - t'$; $L(\tau_{\mu}) = 2.35\gamma_c(3\tau_{\mu})^3\psi(3\tau_{\mu})/2$, where γ_c is calculated using $t_n - 1/2$.
2. Obtain the discretized spectrum: $A(\tau_{\mu}) = L(\tau_{\mu}) \ln 10 / E(t_n - 1/2)$, and calculate $\beta_{\mu} = e^{-\Delta t/\tau_{\mu}}$, $\lambda_{\mu} = \tau_{\mu}(1 - \beta_{\mu})/\Delta t$, $D_{\mu} = [A(\tau_{\mu})(1 - \lambda_{\mu})]^{-1}$. The effective modulus then is $E^{n-1}(t_{n-1/2}) = E^{-1}(t_{n-1/2}) + \sum_{\mu=1}^N D_{\mu}^{-1}$.
3. Calculate the creep strain increment: $\Delta\epsilon'' = \sum_{\mu=1}^N (1 - \beta_{\mu})\gamma_{\mu}^{(n-1)}$. The stress-strain relation for this integration point to be supplied to ABAQUS: $\Delta\sigma = \epsilon''(t_n - 1/2) \mathbf{D}(\Delta\epsilon - \Delta\epsilon'')$.
4. Update the internal variables $\gamma_{\mu}^{(n)} = \lambda_{\mu}\Delta\sigma D_{\mu}^{-1} + \beta_{\mu}\gamma_{\mu}^{(n-1)}$, and go to the next time step.

To check programming, the following results should be obtained: For $\gamma_c = 1.25(t')^{-0.118}$, $E_e = E_{28}\sqrt{t}/(4 + 0.85t)$ where $E_{28} = 30$ GPa, and $\sigma = 1$ MPa applied at $t_0 = 7$ days, the results are $\epsilon = 4.92 \times 10^{-5}$ for $t = 8$ days; $\epsilon = 9.68 \times 10^{-5}$ for $t = 100$ days; $\epsilon = 0.00012$ for $t = 1,000$ days and $\epsilon = 0.000129$ for $t = 10,000$ days. These are almost the same results as those obtained directly from the ACI formula.

Acknowledgments

Financial support from the U.S. Department of Transportation through Grant No. 0740-357-A222 from the Infrastructure Technology Institute of Northwestern University is gratefully acknowledged. Thanks are due to Khaled Shawwaf of Dywidag Systems International USA, Bolingbrook, Illinois, for providing valuable information on the analysis, design, and investigations of the Koror-Babeldaob Bridge; to Man-Chung Tang and Mirek Olmer of T.Y. Lin International, San Francisco; to Brian McDonald of Exponent Failure Analysis Associates, Menlo Park, California; and to Raymond Zelinski, Caltrans, for some additional valuable comments; and to Yasumitsu Watanabe of Shimizu Co., Tokyo, and Lukáš Vráblík of CTU Prague for graciously providing the data on four Japanese bridges and on the Děčín Bridge.

References

- ABAM Engineers Inc. (ABAM). (1993). "Basis for design, Koror-Babeldaob bridge repairs." *Rep. submitted to Bureau of Public Works*, Koror, Republic of Palau, October.
- Abdel-Samad, S. R., Wright, R. N., and Robinson, A.-R. (1968). "Analysis

- of box girders with diaphragms." *J. Struct. Div., Proc. ASCE*, 94(ST10), 2231-2255.
- ACI Committee 209 (ACI). (1971). "Prediction of creep, shrinkage and temperature effects in concrete structures." *ACI-SP27*, Farmington Hills, MI, 51-93.
- ACI Committee 209 (ACI). (2008). "Guide for modeling and calculating shrinkage and creep in hardened concrete." *ACI Report 209.2R-08*, Farmington Hills, MI.
- Bažant, Z. P. (1967). "Linear creep problems solved by a succession of generalized thermoelasticity problems." *Acta Technica ČSAV*, 12, 581-594.
- Bažant, Z. P. (1968a). "Langzeitige Durchbiegungen von Spannbetonbrücken infolge des Schwingkriechens unter Verkehrslasten. (Long-time deflections of prestressed concrete bridges due to cyclic creep under traffic loads)." *Beton und Stahlbetonbau*, 63, 282-285.
- Bažant, Z. P. (1968b). "On causes of excessive long-time deflections of prestressed concrete bridges. Creep under repeated live load." *Inženýrské Stavby*, 16, 317-320 (in Czech).
- Bažant, Z. P. (1971). "Numerically stable algorithm with increasing time steps for integral-type aging creep." *Proc. First Int. Conf. on Struct. Mech. in Reactor Tech. (SMIRT-1)*, T. A. Jaeger, ed., Vol. 4, Part H, Bundesanstalt für Materialforschung und-prüfung (BAM), Berlin, 119-126.
- Bažant, Z. P. (1975). "Theory of creep and shrinkage in concrete structures: A précis of recent developments." *Mechanics Today*, S. Nemat-Nasser, ed., Vol. 2, Pergamon Press, Oxford, U. K., 1-93.
- Bažant, Z. P. (1982). "Mathematical models of nonlinear behavior and fracture of concrete." *Nonlinear numerical analysis of reinforced concrete*, L. E. Schwer, ed., ASME, New York, 1-25.
- Bažant, Z. P. (2000). "Criteria for rational prediction of creep and shrinkage of concrete." *ACI SP-194*, A. Al-Manaseer, ed., ACI, Farmington Hills, MI, 237-260.
- Bažant, Z. P., and Baweja, S. (1995). "Creep and shrinkage prediction model for analysis and design of concrete structures: Model B3." *Mater. Struct.*, 28(6), 357-367.
- Bažant, Z. P., and Baweja, S. (2000). "Creep and shrinkage prediction model for analysis and design of concrete structures: Model B3." *ACI SP-194*, A. Al-Manaseer, ed., ACI, Farmington Hills, MI, 1-83.
- Bažant, Z. P., Hauggaard, A. B., Baweja, S., and Ulm, F.-J. (1997). "Microprestress-solidification theory for concrete creep. I. Aging and drying effects." *J. Eng. Mech.*, 123(11), 1188-1194.
- Bažant, Z. P., and Kaplan, M. F. (1996). *Concrete at high temperatures: Material properties and mathematical models*, Longman (Addison-Wesley), London.
- Bažant, Z. P., and Kim, J.-K. (1992). "Improved prediction model for time-dependent deformations of concrete: Part 5-Cyclic load and cyclic humidity." *Mater. Struct.*, (RILEM, Paris), 25(147), 163-169.
- Bažant, Z. P., and Li, Y. N. (1997). "Cohesive crack with rate-dependent opening and viscoelasticity: I. Mathematical model and scaling." *Int. J. Fract.*, 86(3), 247-265.
- Bažant, Z. P., and Panula, L. (1979). "Practical prediction of time-dependent deformations of concrete: Part 6-Cyclic creep, nonlinearity and statistical scatter." *Mater. Struct.*, (RILEM, Paris), 12, 175-183.
- Bažant, Z. P., and Prasannan, S. (1988). "Solidification theory for aging creep." *Cement Concr. Res.*, 18(6), 923-932.
- Bažant, Z. P., and Prasannan, S. (1989a). "Solidification theory for concrete creep: I. Formulation." *J. Eng. Mech.*, 115(8), 1691-1703.
- Bažant, Z. P., and Prasannan, S. (1989b). "Solidification theory for concrete creep: II. Verification and application." *J. Eng. Mech.*, 115(8), 1704-1725.
- Bažant, Z. P., Sener, S., and Kim, J. K. (1987). "Effect of cracking on drying permeability and diffusivity of concrete." *ACI Mater. J.*, 84, 351-357.
- Bažant, Z. P., and Xi, Y. (1995). "Continuous retardation spectrum for solidification theory of concrete creep." *J. Eng. Mech.*, 121(2), 281-288.
- Benscoter, S. U. (1954). "A theory of torsion bending for multi-cell beams." *J. Appl. Mech. ASME*, 21(1), 25-34.
- Berger/ABAM Engineers Inc. (Berger/ABAM). (1995). "Koror-Babeldaob Bridge modifications and repairs." *Internal rep.*, October 1995, Federal Way, WA.
- Brooks, J. J. (1984). "Accuracy of estimating long-term strains in concrete." *Mag. Concr. Res.*, 36(128), 131-145.

- Brooks, J. J. (2005). "30-year creep and shrinkage of concrete." *Mag. Concr. Res.*, 57(9), 545–556.
- Buckler, J. D., and Scribner, C. F. (1985). "Relaxation characteristics of prestressing strand." *Engineering Studies, Rep. No. UILU-ENG-85-2011*, Univ. of Illinois, Urbana, IL.
- Comité Euro-International du Béton (CEB). (1990). *CEB-FIB Model Code 1990: Model Code for Concrete Structures*, Thomas Telford, London.
- Cottrell, A. H. (1964). *The mechanical properties of matter*, Wiley, New York.
- DRC Consultants Inc. (DRC). (1996). "Koror-Babelthuap bridge: Force distribution in bar tendons." *Internal Rep.*, February 1990, New York.
- Fédération Internationale de Béton (FIB). (2010). *Draft of FIB Model Code*, Lausanne, Switzerland.
- Gaede, K. (1962). "Versuche über die Festigkeit und die Verformungen von Beton bei Druck-Schwellbeanspruchung." *Deutscher Ausschluß für Stahlbeton*, Vol. 144, W. Ernst & Sohn, Berlin.
- Hirst, G. A., and Neville, A. M. (1977). "Activation energy of concrete under short-term static and cyclic stresses." *Mag. Concr. Res.*, 29(98), 13–18.
- Japan International Cooperation Agency (JICA). (1990). "Present condition survey of the Koror-Babelthuap bridge." *Internal Rep.*, February 1990, Tokyo.
- Jirásek, M., and Bažant, Z. P. (2002). *Inelastic analysis of structures*, Wiley, London.
- Kern, E., and Mehmel, A. (1962). "Elastische und plastische Stauchungen von Beton infolge Druckschwell- und Standbelastung." *Deutscher Ausschluß für Stahlbeton*, Vol. 153, W. Ernst & Sohn, Berlin.
- Křístek, V., Bažant, Z. P., Zich, M., and Kohoutková (2006). "Box girder deflections: Why is the initial trend deceptive?." *ACI SP-194*, Farmington Hills, MI, 237–260.
- Křístek, V., Vráblík, L., and Bažant, Z. P., Li, G.-H., and Yu, Q. (2008). "Misprediction of long-time deflections of prestressed box girders: Causes, remedies and tendon layout." *Proc., CONCREEP-8 (8th Int. Conf. on Creep, Shrinkage and Durability of Concrete, Ise-Shima, Japan)*, T. Tanabe, ed., CRC Press/Balkema, London, 1291–1295.
- Magura, D. D., Sozen, M. A., and Siess, C. P. (1964). "A study of stress relaxation in prestressing reinforcement." *PCI J.*, 9(2), 13–57.
- Malcolm, D. J., and Redwood, R. G. (1970). "Shear lag in stiffened box girders." *J. Struct. Div., Proc. ASCE*, 96(ST7), 1403–1419.
- Mamillan, M., and Lellan, M. (1970). "Le fluage de béton." *Annale Inst. Tech. Bat. Trav. Publics (Supp.)*, 23(270), 7–13.
- Navrátil, J. (1998). "Improvement of accuracy of prediction of creep and shrinkage of concrete." *Stavební Obzor*, 2, 44–50 (in Czech).
- Nilson, A. H. (1987). *Design of prestressed concrete*, 2nd Ed., Wiley, New York.
- Reissner, E. (1946). "Analysis of shear lag in box beams by the principle of minimum potential energy." *Q. Appl. Math.*, 4(3), 268–278.
- Richtlinien (1973). "Für die Bemessung und Ausführung Massiver Brücken." *German Standards, Substitute for DIN 1075 Deutsches Institut für Normung e. V. (DIN)*, Berlin.
- RILEM Committee TC-69 (RILEM). (1988). "State of the art in mathematical modeling of creep and shrinkage of concrete." *Mathematical modeling of creep and shrinkage of concrete*, Z. P. Bažant, ed., Wiley, New York, 57–215.
- Suter, G. T., and Mickleborough, N. C. (1975). "Creep of concrete under cyclically loading dynamic loads." *Cement Concr. Res.*, 5(6), 565–576.
- Tschoegl, N. W. (1989). *The phenomenological theory of linear viscoelastic behavior: An introduction*, Springer Verlag, Berlin.
- T. Y. Lin International. (1996). "Collapse of the Koror-Babelthuap Bridge." *Internal Rep.*, San Francisco.
- Whaley, C. P., and Neville, A. M. (1973). "Non-elastic deformation of concrete under cyclic compression." *Mag. Concr. Res.*, 25(84), 145–154.